PLOS PATHOGENS

RESEARCH ARTICLE

N-acetylglucosamine supplementation fails to bypass the critical acetylation of glucosamine-6-phosphate required for *Toxoplasma gondii* replication and invasion

María Pía Alberione[1], Víctor González-Ruiz[2¤], Olivier von Rohr[3], Serge Rudaz[2], Dominique Soldati-Favre[3], Luis Izquierdo[1,4]*, Joachim Kloehn[3]*

1 Barcelona Institute for Global Health (ISGlobal), Hospital Clínic-University of Barcelona, Barcelona, Spain, **2** School of Pharmaceutical Sciences, University of Geneva, Geneva, Switzerland, **3** Department of Microbiology and Molecular Medicine, University of Geneva, Geneva, Switzerland, **4** CIBER de Enfermedades Infecciosas (CIBERINFEC), Barcelona, Spain

¤ Current address: Centro de Metabolómica y Bioanálisis (CEMBIO), Facultad de Farmacia, Universidad San Pablo-CEU, CEU Universities, Boadilla del Monte, Madrid, Spain
* luis.izquierdo@isglobal.org (LI); Joachim.kloehn@unige.ch (JK)

OPEN ACCESS

Citation: Alberione MP, González-Ruiz V, von Rohr O, Rudaz S, Soldati-Favre D, Izquierdo L, et al. (2024) *N*-acetylglucosamine supplementation fails to bypass the critical acetylation of glucosamine-6-phosphate required for *Toxoplasma gondii* replication and invasion. PLoS Pathog 20(6): e1011979. https://doi.org/10.1371/journal.ppat.1011979

Editor: Laura J. Knoll, University of Wisconsin Medical School, UNITED STATES

Received: January 17, 2024

Accepted: June 3, 2024

Published: June 20, 2024

Data Availability Statement: All data pertaining to this study is made available in this manuscript. Raw data was deposited on the Yareta repository operating under the FAIR principles and can be accessed under: 10.26037/yareta:kzx5tn5dincynif3hk44jvhmiy.

Funding: This work is supported by the Swiss National Science Foundation's Indo-Swiss Joint Research Programme (ISJRP) IZLIZ3_200277

Abstract

The cell surface of *Toxoplasma gondii* is rich in glycoconjugates which hold diverse and vital functions in the lytic cycle of this obligate intracellular parasite. Additionally, the cyst wall of bradyzoites, that shields the persistent form responsible for chronic infection from the immune system, is heavily glycosylated. Formation of glycoconjugates relies on activated sugar nucleotides, such as uridine diphosphate *N*-acetylglucosamine (UDP-GlcNAc). The glucosamine-phosphate-*N*-acetyltransferase (GNA1) generates *N*-acetylglucosamine-6-phosphate critical to produce UDP-GlcNAc. Here, we demonstrate that downregulation of *T. gondii* GNA1 results in a severe reduction of UDP-GlcNAc and a concomitant drop in glycosylphosphatidylinositols (GPIs), leading to impairment of the parasite's ability to invade and replicate in the host cell. Surprisingly, attempts to rescue this defect through exogenous GlcNAc supplementation fail to completely restore these vital functions. In depth metabolomic analyses elucidate diverse causes underlying the failed rescue: utilization of GlcNAc is inefficient under glucose-replete conditions and fails to restore UDP-GlcNAc levels in GNA1-depleted parasites. In contrast, GlcNAc-supplementation under glucose-deplete conditions fully restores UDP-GlcNAc levels but fails to rescue the defects associated with GNA1 depletion. Our results underscore the importance of glucosamine-6-phosphate acetylation in governing *T. gondii* replication and invasion and highlight the potential of the evolutionary divergent GNA1 in Apicomplexa as a target for the development of much-needed new therapeutic strategies.

awarded to DSF; by the Carigest SA (https://carigest.ch/) to DSF; by the Novartis Foundation for Medical Biological Research (22C164 awarded to JK). The Barcelona Institute for Global Health (ISGlobal) is supported by the Spanish Ministry of Science and Innovation through the Centro de Excelencia Severo Ochoa 2019-2023 Program (CEX2018-000806-S). The work is also supported by the Generalitat de Catalunya through the CERCA Program (https://cerca.cat). This work is part of the ISGlobal's Program on the Molecular Mechanisms of Malaria, partially supported by the Fundación Ramón Areces (https://www.fundacionareces.es). LI received support by PID2019-110810RB-I00 and PID2022-137031OB-I00 grants from the Spanish Ministry of Science & Innovation. The work is supported by a FI Fellowship from the Generalitat de Catalunya supported by Secretaria d'Universitats i Recerca de la Generalitat de Catalunya and Fons Social Europeu (2021 FI_B 00470 to MPA). MPA also received support from an EMBO Scientific Exchange Grant (9474). The funders had no role in study design, data collection and analysis, decision to publish, or preparation of the manuscript.

Competing interests: The authors have declared that no competing interests exist.

Author summary

Toxoplasma gondii, *Plasmodium*, and *Cryptosporidium* spp. pose serious threats to human health. *T*. *gondii*, an intracellular and opportunistic pathogen, effectively avoids the host immune defences by forming long-lasting tissue cysts. Finding potent drugs to eliminate these persisting parasites remains a challenge.

The glucosamine-phosphate-*N*-acetyltransferase (GNA1) catalyses a critical key step in the production of activated sugar nucleotides to build glycoconjugates essential for various functions in the cell. In *P*. *falciparum*, this enzyme has been identified as a potential target for antimalarial drugs.

In this study, we explored the importance of this pathway in *T*. *gondii* and discovered that these sugar-containing compounds play a vital role in the parasite's ability to invade and replicate in host cells–crucial processes for its survival and ability to cause disease. Intriguingly, unlike some organisms that can bypass the pathway, *T*. *gondii* relies critically on glucosamine-6-phosphate acetylation. This reliance sheds light on the parasite's distinct metabolic properties and highlights the pathway's potential as a target for new therapeutic strategies.

Introduction

The phylum of Apicomplexa groups a vast number of obligate intracellular parasites, some of which pose a considerable threat to human health. The most ubiquitous apicomplexan, *Toxoplasma gondii*, causes disease in immunocompromised individuals [1,2], as well as abortions, stillbirths, fetal death, retinal lesions or long-term disabling sequelae in congenitally infected children [3,4]. At present, there is no vaccine that prevents toxoplasmosis, and the available treatments are associated with a range of shortcomings including high cost, toxicity and rising resistance [5]. In the accidental human host, *T*. *gondii* manifests in two distinct stages: the fast-replicating tachyzoite, responsible for acute disease and the slow replicating bradyzoite, which persists encysted within muscle cells and neurons throughout the lifetime of its host [6]. These persistent parasites constitute a reservoir, that can reactivate causing life-threatening acute toxoplasmosis when the infected individual becomes immunocompromised. The inability to eradicate the parasite's latent form, combined with the emergence of parasites that are resistant to existing drugs against acute toxoplasmosis, underscores the pressing need for novel therapeutic strategies [5].

The endomembrane system of *T*. *gondii* is rich in glycoconjugates which play fundamental roles in infectivity, survival, and virulence [7]. Several glycan structures have been characterized in *T*. *gondii* including *N*-glycans [8], *O*-glycans [9–13], *C*-mannose [9,14], GPI-anchors [15,16], and others [7]. These glycans serve various critical functions from invasion to O_2 sensing and nutrient storage, hence contributing to the overall virulence of the parasite [7]. Additionally, glycans are critical components of the bradyzoite cyst wall and the disruption of their formation impairs the parasite's ability to persist [17,18].

The *de novo* synthesis of glycans relies on activated sugar nucleotides. Uridine diphosphate *N*-acetylglucosamine (UDP-GlcNAc) serves as a donor by GlcNAc-dependent glycosyltransferases for the synthesis of *N*-glycans, glycosylphosphatidylinositol (GPI) -anchors, glycoinositolphospholipids (GIPLs), and for the glycosylation of other protein acceptors. Given the critical roles of these structures for infectivity of tachyzoites [7,8,16,19], and bradyzoite survival and replication [17,18], the biosynthesis route of UDP-GlcNAc is a plausible target for

intervention against acute toxoplasmosis and for eradication the chronic infection. GNA1, the enzyme catalysing the acetylation of glucosamine-6-phosphate (GlcN6P) is considered a promising drug target in Apicomplexa. This is attributed to its independent evolutionary origin, unique sequence features [20], and established essentiality for the intraerythrocytic development of *Plasmodium falciparum* [21].

In *T. gondii*, a genome-wide CRISPR fitness screen underscored the significance of UDP-GlcNAc biosynthesis for the parasite, classifying several genes encoding for enzymes involved in the amino sugar synthesis pathway as fitness-conferring [22,23]. Unexpectedly, however, this study predicted GNA1 to be dispensable for *T. gondii*, even though the upstream and downstream enzymes were classified as highly fitness-conferring [23].

Here we demonstrate the critical role of GNA1 for *T. gondii*, revealing that its downregulation leads to a reduction in GPI anchors that impairs invasion and replication within its host cell. Intriguingly, defects in GNA1 cannot be overcome by GlcNAc salvage. Targeted metabolomic analyses revealed that GlcNAc salvage is inefficient in glucose-replete conditions. In contrast, GlcNAc is effectively salvaged in glucose-deplete conditions, but fails to rectify the defects associated with the disruption of the pathway. These findings highlight the potential of GNA1 as a drug target to combat toxoplasmosis.

Results

GNA1 is highly fitness-conferring for *T. gondii*, contradicting the prediction from a genome-wide fitness screen

T. gondii expresses several glycan structures akin to other eukaryotic cells, with few noteworthy characteristics (Fig 1A). The synthesis of GPI-anchors, *N*-glycans and *O*-glycans requires as donor substrate UDP-GlcNAc, or UDP-GalNAc. The latter can be synthesised from UDP-GlcNAc via GalE [7], a UDP-Glc/UDP-Gal epimerase. In the amino sugar biosynthesis pathway, the glucosamine 6-phosphate *N*-acetyltransferase, GNA1, catalyses the acetylation of GlcN6P (Fig 1B). Although *T. gondii* has been shown to critically rely on several glycan structures [7–9], *Tg*GNA1 (TGGT1_243600) was assigned a positive fitness score (+1.41) in a genome-wide fitness screen [23], indicating its potential dispensability (Fig 1C). This is unexpected considering the crucial role of GNA1 in other organisms [24], including *P. falciparum* [21]. Additionally, enzymes acting either downstream or upstream of GNA1 were assigned negative fitness scores in *T. gondii*, highlighting their critical role for parasite replication and development [23].

Examination of the nanopore sequencing data on ToxoDB [25,26] revealed two major GNA1 transcripts, with the shorter, more prevalent transcript, only covering a portion of the predicted protein coding sequence. In addition to the predicted GNA1 protein coding sequence, which encodes a putative protein of 55.5 kDa, four additional in-frame open reading frames were identified downstream. These could give rise to GNA1 proteins of various reduced sizes (45.5, 21.0, 17.2 and 16.7 kDa) [25] (Figs 2A and S1A). Critically, the acetyltransferase domain is located near the C-terminus and is present in all five putative isoforms. Consequently, all proteins, including the shortest version, could potentially be catalytically active. These shorter GNA1 isoforms may explain the unexpected positive fitness score for GNA1 [23]. Concordantly, out of the ten single guide RNAs (sgRNAs) used to target GNA1 in the genome wide fitness screen [25,26], four bind near the extended N-terminus, only present in the longest isoform of GNA1 (guides sgTGGT1_243600_5, _6, _9 and _10; average fitness score +1.02), while three bind close to the C-terminus of GNA1, disrupting all potential isoforms, (guides sgTGGT1_243600_2, _3, and _4; average fitness score: -7.50) (Figs 2A and S1A). Notably, the published phenotype score is calculated by averaging the value of the top

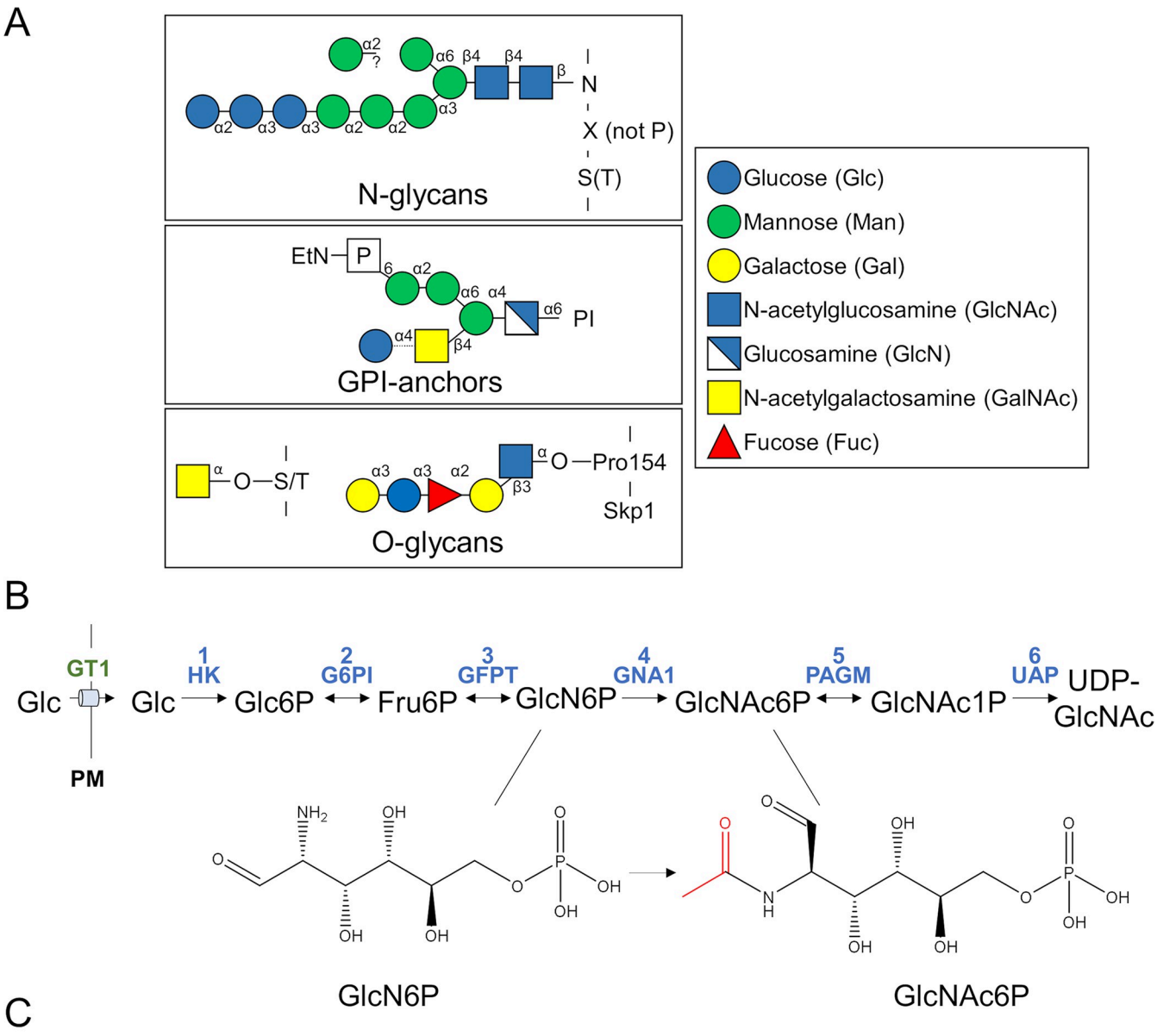

Step	Enzyme name	Enzyme number	*T. gondii*			*P. falciparum* homologues	
			ID number	FS	hLOPIT	ID number	MFS
1	Hexokinase (HK)	EC 2.7.1.1	TGGT1_265450	-1.37	cytosol	PF3D7_0624000	-2.565
2	Glucose-6-phosphate isomerase (G6PI)	EC 5.3.1.9	TGGT1_283780	-2.52	cytosol	PF3D7_1436000	-3.115
3	Glucosamine-fructose-6-phosphate aminotransferase (GFPT)	EC 2.6.1.16	TGGT1_231350	-4.57	mitochondrion - soluble	PF3D7_1025100	-3.187
4	Glucosamine-phosphate N- acetyltransferase (GNA1)	EC 2.3.1.4	TGGT1_243600	1.41	cytosol	PF3D7_0629000	-3.365
5	Phosphoacetylglucosamine mutase (PAGM)	EC 5.4.2.3	TGGT1_264650	-2.94	cytosol	PF3D7_1130000	-2.855
6	UDP-N-acetylglucosamine pyrophosphorylase (UAP)	EC 2.7.7.23	TGGT1_264780	-5.22	nucleolus	PF3D7_1343600	-3.188

Fig 1. Glycans and UDP-GlcNAc synthesis in *T. gondii*. A) Proteins of the secretory pathway of *Toxoplasma gondii* are commonly modified as *N*-glycans, *O*-glycans or GPI-anchored. The typical glycan structures in *T. gondii* are shown, as well as the modification of Skp1, which harbours a specific *O*-glycosylation [73]. Free, non-protein bound GPIs (glycoinositolphospholipids, GIPLs) are distinguished from GPI anchors by a Glc residue linked to GalNAc (see dashed line). **B)** The activated sugar nucleotide UDP-GlcNAc is synthesised from glucose in six conserved enzymatic reactions, with the glucosamine-phosphate *N*-acetyltransferase (GNA1) converting glucosamine-6-phosphate (GlcN6P) to *N*-acetylglucosamine-6-phosphate (GlcN6P) **C)** Overview of *T.*

gondii enzymes in UDP-GlcNAc synthesis, listing their names, accession number (ID) [25], fitness score (FS) [23] and putative localisation (hLOPIT) [74], as well as the accession number [75] and mutagenesis fitness score (MFS) [76] in the related *Plasmodium falciparum* parasite. Abbreviations: PI: phosphatidylinositol; EtN: ethanolamine; GT1: glucose transporter 1; PM: plasma membrane; Fru, fructose; PI, phosphatidylinositol; GPI, glycosylphosphatidyl inositol; UDPGlcNAc, uridine diphosphate *N*-acetylglucosamine. Other abbreviations, see panel A and C.

https://doi.org/10.1371/journal.ppat.1011979.g001

five scoring guides to mitigate the impact of stochastic losses, resulting in the positive fitness score for GNA1 [23]. Given the likely existence of diverse isoforms, the assigned fitness score probably does not reflect the importance that GNA1 may play for *T. gondii*, prompting further investigation of the enzyme.

To examine the localization and function of GNA1 in *T. gondii* (TGGT1_243600), the endogenous locus was edited using CRISPR/Cas9 [23,27]. A Ty epitope tag and a mini auxin inducible degron (mAID) domain were simultaneously fused to the C-terminus of GNA1 in parasites stably expressing the auxin receptor transport inhibitor response 1 (TIR1) from *Oryza sativa* (RH-TIR1) [28,29]. The hypoxanthine-xanthine-guanine phosphoribosyl transferase (*hxgprt*) resistance cassette was inserted, for selection of positive transfectants (S1B Fig) [30]. The mAID domain enables rapid and efficient downregulation of the protein of interest via proteasomal degradation upon addition of auxin (indole 3-acetic acid, IAA) [29]. Successful integration of the construct at the *gna1* locus in a clonal population was confirmed by genomic PCR (S1C Fig), using primers listed in S1 Table. GNA1-mAID-Ty exhibited a punctate localization by immunofluorescence assay (IFA), throughout the parasite's cytosol (Fig 2B). Subsequently, downregulation of GNA1 was assessed by western blot (2, 4- and 18-hours IAA treatment, Fig 2C) and by IFA (18-hours IAA treatment, Fig 2D), confirming efficient depletion of GNA1 within 2–4 hours of IAA treatment. Interestingly, the western blot revealed several bands between approximately 30–80 kDa for GNA1-mAID-Ty (Fig 2C), all of which were efficiently downregulated at similar rates upon addition of IAA. As outlined above, up to five GNA1 isoforms may exist, with molecular weights ranging from 29.7–68.5 kDa, including the tag. These observations suggest that full length GNA1 as well as shorter isoforms (Figs 2A and S1A) are synthesised, although partial degradation cannot be excluded and may contribute to the bands observed at lower molecular weights.

The significance of GNA1 for the parasite's lytic cycle was assessed by plaque assay. Downregulation of GNA1 prevented the formation of plaques of lysis (Fig 2E), indicating that GNA1 is needed for one or several steps of the lytic cycle. An intracellular growth assay revealed a significant impact of GNA1 depletion on the replication rate, with the average number of parasites during 24 hours of growth decreasing from 6.5 in the controls to 4.2 following 36 hours of IAA treatment (Fig 2F).

These results reveal a critical function of GNA1 for intracellular growth and the overall lytic cycle of *T. gondii*, consistent with the importance of glycoconjugates. Taken together, the data suggest that two major mRNA transcripts are generated for GNA1, yielding up to five protein isoforms, all of which contain the acetyltransferase domain and therefore can be potentially catalytically active. The extended N-terminus in the longer isoform is likely dispensable [23]. Whether it holds a regulatory function in other life cycle stages remains unknown. Crucially, loss of the GNA1 acetyltransferase domain is detrimental to *T. gondii*.

GNA1 is active and critical for UDP-GlcNAc synthesis in *T. gondii*

To examine if the UDP-GlcNAc biosynthesis pathway is active in intra- and extracellular *T. gondii*, TIR1 parasites were cultured intracellularly for 24 hours in medium containing 10 mM uniformly ^{13}C-labelled glucose (U-$^{13}C_6$-Glc) or extracted and purified extracellular parasites were incubated for three hours in medium containing heavy Glc. Post-incubation, the

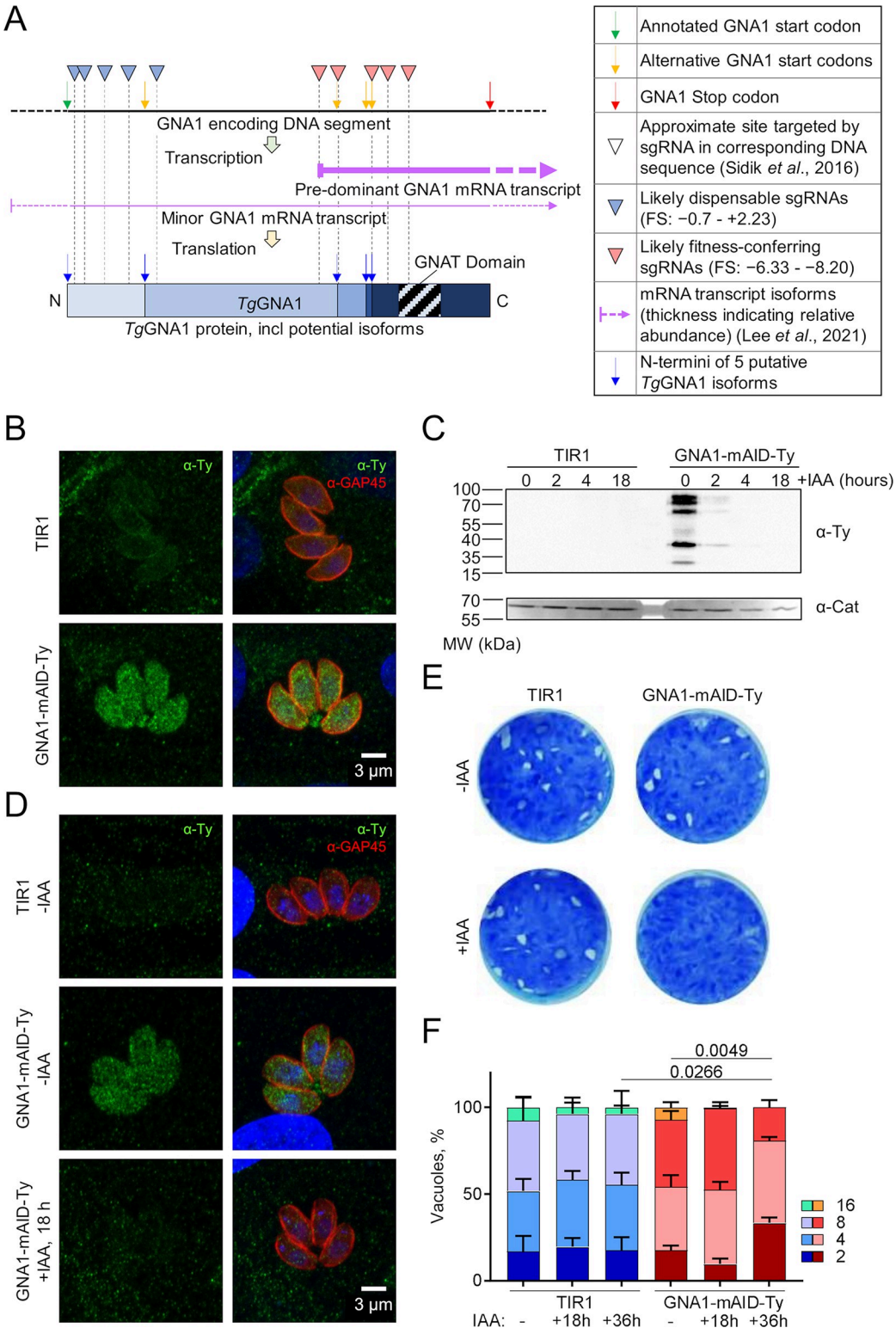

Fig 2. GNA1 is essential for *T. gondii*. A) Cartoon schematic depicting the DNA segment and transcripts encoding GNA1 as well as the resulting protein(s). The approximate sites targeted by the single guide RNAs (sgRNAs) in the genome-wide fitness screen are shown. Dotted vertical lines illustrate where the sgRNAs impact on the resulting transcripts and protein. Positions of the varying in frame start codons and the resulting GNA1 isoforms are depicted. **B)** Immunofluorescence assay (IFA) showing the pellicle marker GAP45 and Ty signal in GNA1-mAID-Ty parasite line and

its parental line (TIR1). **C)** Western blot revealing the signal of Ty-tagged GNA1 and TIR1 at different time points of auxin (IAA) treatment. **D)** IFA showing Ty signal in GNA1-mAID-Ty parasites in the absence of IAA and 18 hours after IAA treatment. **E)** Lysis plaques formed over one week of TIR1 and GNA1-mAID-Ty parasite cultivation in the presence or absence of IAA. **F)** Growth assay of TIR1 and GNA1-mAID-Ty parasites showing the number of parasites per vacuole after 24 hours of growth and varying durations of IAA treatment. B-E show representative images of three independent experiments. F shows the means and standard deviation (error bars) from representative data of one of three independent biological replicates averaging technical triplicates. p-values are given comparing the average number of parasites by two-sided Student's t-test, between the indicated conditions. Abbreviations: MW, molecular weight; CAT, catalase.

https://doi.org/10.1371/journal.ppat.1011979.g002

metabolism was quenched, parasites were harvested, and metabolites extracted. Gas chromatography-mass spectrometry (GC-MS) was employed following derivatization of the sugars to assess the extent of label incorporation into *N*-acetylglucosamine-6-phosphate (GlcNAc6P) (Figs 3A and S2). Labelling was quantified in a fragment (*m/z* 357), which contains the two carbons proximal to the phosphate group and can be found in most sugar-phosphates, including glucose-6-phosphate (Glc6P) and GlcNAc6P (S2A–S2C Fig). The fragment shifts to *m/z* 359 upon incorporation of heavy carbons from U-$^{13}C_6$-Glc (S2D–S2J Fig). Synthesis of GlcNAc6P from labelled Glc was observed in both parasite stages, reaching 88.8% and 25.5% labelling in intra- and extracellular parasites, respectively (Fig 3A). These findings suggest an active UDP-GlcNAc biosynthesis pathway from Glc in both intra- and extracellular *T. gondii*.

To assess the critical role of GNA1 in the pathway, TIR1 and GNA1-mAID-Ty parasites were untreated or pre-treated with IAA for 18 hours and extracellular parasites incubated in medium containing 10 mM U-$^{13}C_6$-Glc. TIR1 –IAA parasites that served as control, were incubated with regular medium containing unlabelled (natural abundance) Glc. After five hours of incubation, parasites were harvested, metabolites extracted, derivatized and analysed by GC-MS in a targeted manner (S2 Fig). Under all tested conditions, Glc6P was detected with incorporation of heavy carbons under ^{13}C-labelling conditions (Fig 3B). GlcNAc6P, the product of GNA1, was detected in all conditions, except in parasites depleted in GNA1 (Fig 3B). Significant levels of labelling were only detected in GlcNAc6P from parasites expressing GNA1 and supplied with U-$^{13}C_6$-Glc. The relative low levels of labelling are consistent with previous studies [31] and likely reflect a reduction of the pathway's activity in extracellular parasites and/or are the result of a dilution of the labelled glucose pool by an unlabelled source, *e.g.*, from the storage polysaccharide amylopectin. While amylopectin is well known to accumulate in bradyzoites [32], it has recently been shown to also be critical for the metabolism of tachyzoites [33].

Given that crucial intermediates such as GlcNAc1P and the product UDP-GlcNAc cannot be detected by GC-MS, we turned to liquid chromatography mass spectrometry (LC-MS/MS) for more sensitive detection of all relevant pathway intermediates. Intracellular parasites were treated with IAA or not for 18 hours, before quenching of the metabolism, parasite harvest, metabolite extraction and analysis. Precursor and product signals obtained for GlcN6P and UDP-GlcNAc are shown in S3A and S3B Fig, respectively, for representative replicates of parasites depleted in GNA1 and the relevant controls. The specific transitions for each metabolite are listed in S2 Table. While fructose-6-phoshate (Fru6P) levels remained unaffected by GNA1 downregulation (GNA1-mAID-Ty +IAA), GlcN6P accumulated dramatically to 91.8-fold higher levels compared to the controls (Fig 3C). In sharp contrast, as observed by GC-MS, GlcNAc6P was markedly reduced (50.9-fold). Similarly, the subsequent metabolites, GlcNAc1P and the product UDP-GlcNAc exhibited reductions of 83.3- and 803.2-fold, respectively (Fig 3C).

Together, these findings reveal that UDP-GlcNAc synthesis is active both in intra- and extracellular *T. gondii* tachyzoites, Moreover, GNA1 plays a critical role in this pathway as its

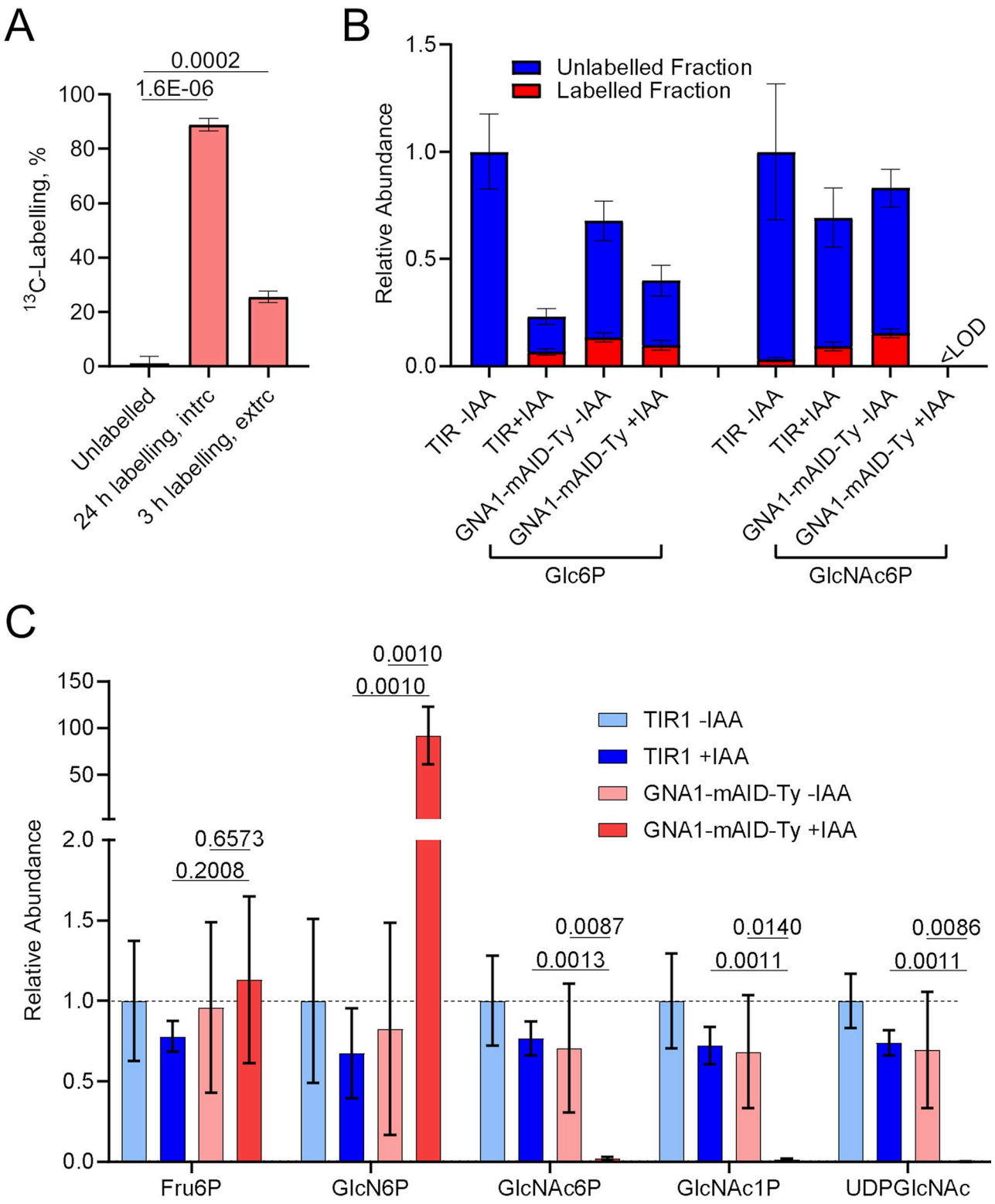

Fig 3. UDP-GlcNAc synthesis is disrupted in *T. gondii* that lack GNA1. A) Percent ^{13}C-labelling in *T. gondii* (TIR1) derived *N*-acetylglucosamine-6-phosphate (GlcNAc6P) in unlabelled parasites (natural abundance) or after incubation of intracellular or extracellular parasites in medium containing U-$^{13}C_6$-glucose for 24 or three hours, respectively. **B)** Relative abundance and fractional ^{13}C-labelling in TIR1 and GNA1-mAID-Ty parasite metabolite extracts, following incubation of extracellular parasites in medium containing U-$^{13}C_6$-glucose for five hours in the absence of auxin (−IAA) or following 18 hours pre-treatment (+IAA). TIR1 −IAA parasites were incubated in medium with natural abundance glucose as an unlabelled

control. Note that metabolites for which the abundance of labelled and unlabelled ions was too low to obtain reliable labelling data were deemed below limit of detection (<LOD, sum of ion intensity <1000 arbitrary units). **C)** Relative metabolite levels in TIR1 and GNA1-mAID-Ty, following no treatment (−IAA) or treatment with IAA for 18 hours during intracellular growth (+IAA). Data plotted show the means and standard deviation of three (A, B) or four (C) independent biological replicates. p-values from two-sided Student's t-tests are given in A and C, comparing the indicated conditions. Abbreviations: Glc6P, glucose-6-phosphate; GlcN6P, glucosamine-6-phosphate; GlcNAc6P, *N*-acetylglucosamine-6-phosphate; Fru6P, fructose-6-phosphate; GlcNAc1P, *N*-acetylglucosamine-1-phosphate; UDPGlcNAc, uridine diphosphate *N*-acetylglucosamine.

https://doi.org/10.1371/journal.ppat.1011979.g003

disruption results in a significant reduction in the activated sugar nucleotide UDP-GlcNAc and an accumulation of its substrate GlcN6P.

GlcNAc supplementation fails to rescue GNA1 deficiency

Efficient bypass of defects in UDP-GlcNAc synthesis through GlcNAc supplementation is well documented in several organisms, including *P. falciparum*, [21,34,35]. GlcNAc can be taken up and phosphorylated by hexokinase, generating GlcNAc6P, effectively circumventing the initial steps of the pathway. To test if exogenous GlcN or GlcNAc supplementation can bypass the function of GNA1 in *T. gondii*, we performed plaque assays with GNA1-mAID-Ty parasites in presence or absence of IAA while supplementing different concentrations of GlcN or GlcNAc. Remarkably, none of the supplementations could rescue the lytic cycle defect observed in parasites depleted in GNA1 (Fig 4A).

We hypothesised that the inability of GlcN or GlcNAc supplementation to rescue the lytic cycle defect in GNA1-depleted parasites could be attributed to various reasons: I) insufficient uptake of GlcNAc by the host cells and/or *T. gondii*, II) incapacity of *T. gondii* hexokinase to phosphorylate GlcNAc or III) inefficient entry of phosphorylated, salvaged GlcNAc into the UDP-GlcNAc synthesis pathway. To explore these possibilities, we incubated purified extracellular parasites in medium without Glc supplemented with $^{13}C_6$-GlcN or $^{13}C_6$-GlcNAc for five hours, before harvesting parasites and extracting metabolites. GNA1-mAID-Ty and TIR1 parasites were pretreated with IAA for 18 hours to deplete GNA1 levels in the GNA1-mAID-Ty strain. TIR1 parasites not treated with IAA (−IAA) were incubated in regular medium with unlabelled (natural abundance) Glc. Remarkably, both amino sugars were efficiently salvaged and utilised by *T. gondii*. $^{13}C_6$-GlcN was salvaged, phosphorylated and acetylated in the controls but as expected, the downregulation of GNA1 prevented the formation of GlcNAc6P from GlcN (Fig 4B). Similarly, exogenous $^{13}C_6$-GlcNAc was efficiently used to generate labelled GlcNAc6P in the control strains (Fig 4C). Parasites deficient in GNA1 were also able to salvage exogenous $^{13}C_6$-GlcNAc and utilised it to generate GlcNAc6P, albeit at significantly lower levels but fully ^{13}C-labelled, consistent with the inability of Glc to contribute to GlcNAc6P formation. These results reveal that *T. gondii* can salvage and utilise GlcNAc, potentially bypassing the need for GNA1.

It is noteworthy that this experiment was conducted with extracellular parasites which were pre-depleted in GNA1 over 18 hours under regular growth conditions, without GlcNAc supplementation. Thus, these parasites were expected to be impaired in their fitness and this measurement may not reflect what occurs during intracellular development and during continuous supplementation. To address this, we cultured intracellular *T. gondii*, TIR1 and GNA1-mAID-Ty parasites under standard culture conditions for 24 hours before changing the culture medium to one of the following 4 conditions for 18 hours prior to parasite harvest: regular medium −IAA; regular medium +IAA; regular medium +IAA supplemented with 10 mM GlcNAc; and medium without Glc +IAA supplemented with additional glutamine and 10 mM GlcNAc. Parasites were harvested while intracellular, removing the medium and quenching parasite metabolism, prior to the harvest of parasites, to exclude any metabolite uptake by extracellular parasites. Metabolites were extracted and analysed by LC-MS/MS (Fig 4D).

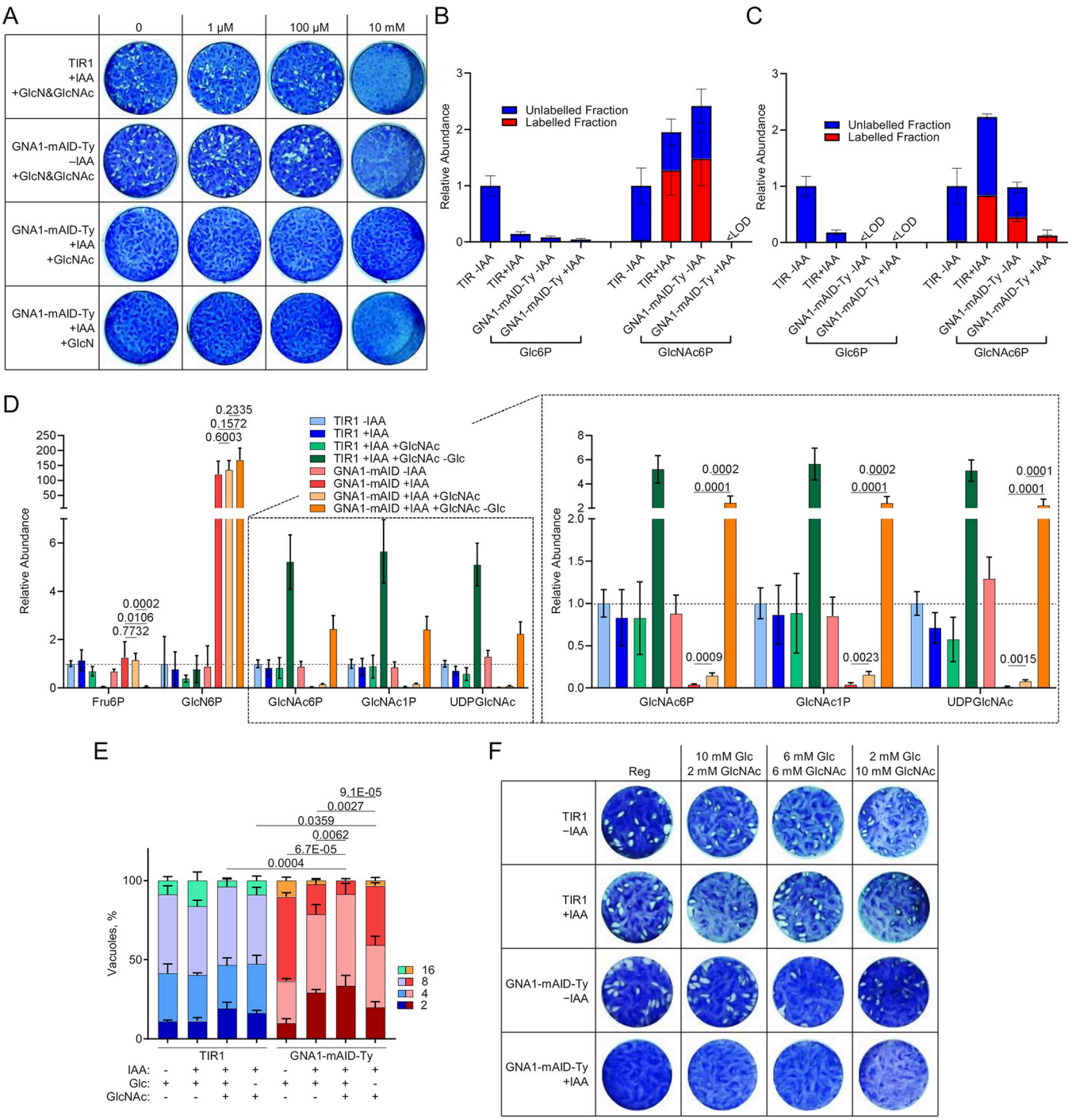

Fig 4. Disruption of *Tg*GNA1 cannot be rescued by GlcNAc supplementation. A) Lysis plaques formed by TIR1 and GNA1-mAID-Ty parasites over one week of growth when treated with auxin (+IAA) or not (–IAA) and supplemented with varying concentrations of glucosamine (GlcN) and/or *N*-acetylglucosamine (GlcNAc) as indicated. **B-C)** Relative metabolite abundance and fractional ^{13}C-labelling in TIR1 and GNA1-mAID-Ty parasite extracts, incubated for five hours extracellularly in medium without glucose and containing U-$^{13}C_6$-glucosamine (**B**) or U-$^{13}C_6$-*N*-acetylglucosamine (**C**) in the absence of IAA or following IAA pre-treatment (+IAA, 18 h). TIR1 –IAA parasites were incubated in medium with natural abundance glucose as an unlabelled control. Note that metabolites for which the abundance of labelled and unlabelled ions was too low to obtain reliable labelling data were deemed below limit of detection (<LOD, sum of ion intensity <1000 arbitrary units). **D)** Relative metabolite levels in TIR1 and GNA1-mAID-Ty parasites, following no treatment (–IAA) or treatment with IAA (+IAA, 18 h) during intracellular growth in the presence or absence of glucose and supplemented with GlcNAc as indicated for the same duration. Overview on the left and detail on the right. **E)** Intracellular growth assay showing the number of parasites per vacuole after 24 hours of growth, treated for 48 hours with IAA, Glc or GlcNAc as indicated. **F)** Lysis plaques formed by TIR1 and GNA1-mAID-Ty parasites over one week of growth

in presence or absence of auxin (IAA) and supplemented with glucose (Glc) or *N*-acetylglucosamine (GlcNAc) in Glc-free medium as indicated. A) shows representative images of three independent experiments. Data plotted in B-E show the means and standard deviation of three (B, C, E) and four (D) independent biological replicates, respectively. p-values from two-sided Student's t-tests are given in D and E, comparing the indicated conditions. p-values in E compare the average number of parasites per vacuole. F) shows a representative image from three independent experiments. Abbreviations: Glc, glucose; GlcNAc, *N*-acetylglucosamine. Other abbreviations, see Fig 3.

https://doi.org/10.1371/journal.ppat.1011979.g004

Remarkably, GlcNAc supplementation had only a marginal impact in the presence of Glc. Although significantly higher than in non-supplemented parasites devoid of GNA1, GlcNAc failed to fully restore UDP-GlcNAc levels, with levels being 13.3-fold lower than in control (TIR1 -IAA) parasites (see detail in Fig 4D). In the absence of Glc, however, GlcNAc was efficiently salvaged and markedly increased UDP-GlcNAc levels, both in TIR1 parasites as well as in parasites deficient of GNA1. Crucially, UDP-GlcNAc levels in GNA1-devoid parasites supplemented with GlcNAc in the absence of Glc were 2.2-fold higher than in control parasites (TIR1 -IAA), suggesting a full rescue of the pathway. Notably, GlcN6P continued to accumulate to levels >100-fold higher in parasites devoid of GNA1, regardless of the presence or absence of Glc in the medium. Since Fru6P levels were markedly down in the absence of Glc, we speculate that the detected GlcN6P is not derived from gluconeogenesis but rather from the deacetylation of GlcNAc, either through deacetylases of the host cell or by the parasite. The generated GlcN6P failed to be converted further in the absence of GNA1, resulting in its accumulation. In summary, this detailed analysis of the pathway under varying conditions reveals efficient GlcNAc salvage but only in the absence of Glc. Under this condition, the function of GNA1 can be bypassed, fully restoring UDP-GlcNAc levels. Whether a potential competition between Glc and GlcNAc happens at the level of uptake by the host or the parasite, or at the level of phosphorylation in the parasite remains unclear.

While GlcNAc supplementation failed to restore the lytic cycle defect in GNA1-depleted parasites in the presence of Glc (Fig 4A), we investigated whether the defects in the parasite's intracellular growth could be rescued by exogenous GlcNAc, both in the presence or absence of Glc. Consistent with the inefficient utilization of GlcNAc in the presence of Glc, GlcNAc supplementation failed to rescue the growth defect in regular medium (Fig 4E). GlcNAc supplementation in the absence of Glc, however, facilitated a significant but modest and incomplete rescue of the intracellular growth rate, following 48 hours of treatment (Fig 4E). Lastly, we explored whether certain ratios of Glc and GlcNAc could potentially rescue parasites depleted in GNA1, by supporting central carbon metabolism (Glc), but facilitating GNA1 bypass (GlcNAc) and potentially alleviating excessive GlcN6P accumulation. Plaque assays were performed with parasites in varying Glc and GlcNAc ratios, however none of the conditions were able to rescue the lytic cycle defect associated with GNA1 downregulation (Fig 4F).

GNA1 is needed for GPI-anchor synthesis critical for host cell invasion by *T. gondii*

The observed impairment of UDP-GlcNAc synthesis in parasites depleted in GNA1 is expected to impair the synthesis of glycans, including GPI-anchors, and free, non-protein-bound GIPLs, which differ from GPI-anchors by a Glc residue linked to GalNAc [7]. GPI-anchored proteins are critical for parasite invasion, contributing to the expression of a series of surface antigens, which play a vital role during host cell attachment [16,36,37]. Additionally, glycosylated proteins have been described to traffic to the apical secretory organelles, playing an essential role in their biogenesis and function [19,38]. To assess if GNA1 is required for the appropriate localization and formation of GPI-anchored proteins, we performed IFAs, evaluating the expression and distribution of the surface antigen 1 (SAG1) [39]. Downregulation of

GNA1 resulted in a drop in SAG1 signal intensity and an aberrant distribution, with the signal commonly accumulating in the residual body (Fig 5A). This abnormal staining was observed in 68.3 and 73.3% of vacuoles following downregulation of GNA1 for 18 or 36 hours, respectively (Fig 5B). Next, we tested whether the downregulation of GNA1 impacts on rhoptry morphology, based on previous reports that a GPI-anchored protein, the *T. gondii* carbonic anhydrase-related protein (TgCA_RP), is needed for rhoptry biogenesis [19]. Indeed, we observed that 59. 0 and 61.5% of parasites displayed abnormal rhoptry morphology following downregulation of GNA1 for 18 and 36 hours, respectively (Fig 5C and 5D). This abnormal morphology was characterized by shorter, diffuse rhoptries, in sharp contrast to the typical club-shaped staining observed in the controls, as revealed when staining with a rhoptry marker (α-ARO antibody) [40]. To investigate if this is a relatively specific defect or if cells devoid of GNA1 exhibit various morphological abnormalities, we assessed the morphology of the apicoplast (S4A Fig) and mitochondrion (S4B Fig), upon GNA1 downregulation for the same duration. The organelles were visualized by IFA using α-CPN60 (chaperonin 60) and α-5F4 (F1 ATPase beta subunit) antibodies, two specific markers for the apicoplast and the mitochondrion, respectively. Both organelles appeared morphologically intact and normal after 18 hours and 36 hours of IAA-treatment.

Next, to confirm if the abnormal SAG1 signal, observed in GNA1-deficient cells, can indeed be attributed to a defect in the synthesis of GPIs, we quantified the relative abundance of GIPLs following downregulation of GNA1 for 36 hours. To this end, parasite lipids were extracted in organic solvent and subjected to methanolysis to hydrolyse monosaccharides off glycan structures found in the organic phase after metabolite extraction. The trimethylsilyl (TMS-) derivatised sugar residues and fatty acid methyl esters were analysed by GC-MS. As previously demonstrated the signal obtained for Man, the most abundant sugar residue in GIPLs, relative to the signal of fatty acids (proxy for total lipids), can serve as a measure for relative GIPL levels [41]. Here, the Man signal was normalised to that of the methyl ester of palmitic acid (FA C16:0), one of the most abundant fatty acids in *T. gondii* [22,31,42]. Notably, the ratio Man signal intensity/FA C16:0 signal intensity decreased 8.5-fold after 36 hours of IAA treatment, consistent with a marked drop in GIPLs and GPI-anchor formation (Fig 5E). We further validated this result and the methodology, by employing an alternative butanol extraction for GIPLs [43], and demonstrating that the Man signal specifically decreased in parasites depleted in GNA1, also when normalised to the signal obtained for other fatty acid methyl esters (C16:1 and C20:1) or to myo-inositol, as a proxy for total lipid and phosphatidylinositol content, respectively (S4C–S4E Fig). As expected, this drop in GPIs and GIPLs caused a severe defect in host cell invasion, with only 26.5% of parasites depleted in GNA1 over 18 hours invading successfully, compared to more than 70% of parasites in all controls (Fig 5F).

To assess if GlcNAc supplementation under Glc-deplete conditions, and the consequent increase in UDP-GlcNAc levels (Fig 4D), could restore GPI-anchor synthesis, GIPL levels were quantified following GlcNAc supplementation. After 18 hours of IAA-treatment and the indicated supplementations, GlcNAc supplementation appeared to elevate relative GIPL levels in TIR1 parasites and led to a slight increase in GIPL levels in GNA1-depleted parasites. However, levels remained markedly lower (~5-fold) compared to control conditions (Fig 5G). Notably, the modest increase in GIPL levels was observed equally under Glc replete and Glc deplete conditions. Relative GIPL levels correlated remarkably well with parasite invasion following 18 hours of treatment with IAA and supplementations as indicated: GlcNAc-supplemented GNA1-depleted parasites demonstrated a significant but still incomplete rescue in their ability to invade host cells (Fig 5H).

Overall, GlcNAc supplementation under Glc deplete conditions fully restored UDP-GlcNAc levels in cells lacking GNA1 (Fig 4D), but this only facilitated a modest and incomplete

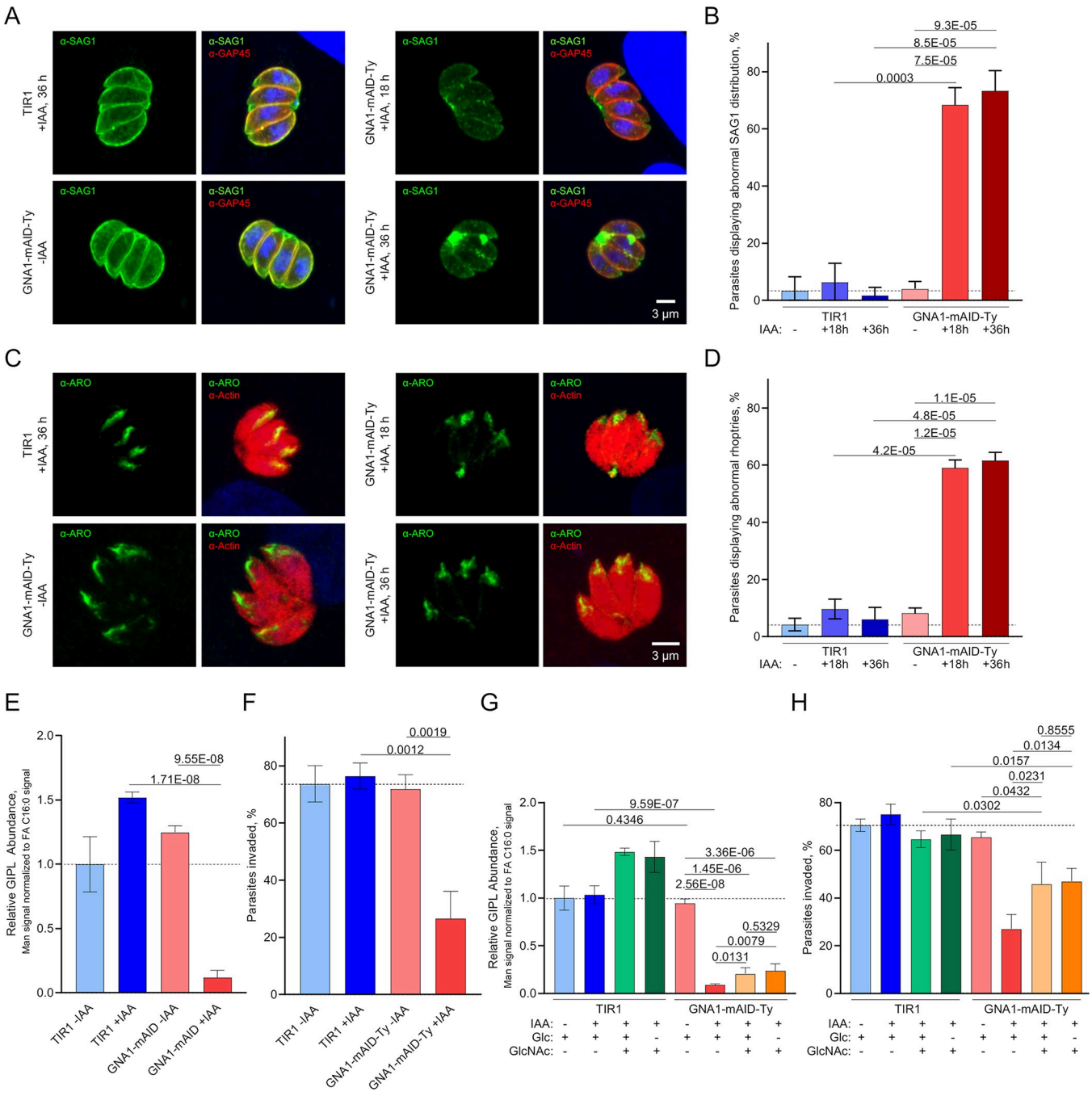

Fig 5. Lack of *Tg*GNA1 disrupts GPI-anchored proteins causing an invasion defect. A) Immunofluorescence assays (IFAs), showing the staining of the pellicle marker GAP45 and the GPI-anchored protein surface antigen 1 (SAG1) in TIR1 and GNA-mAID-Ty parasites after varying durations of auxin (IAA) treatment. **B)** Quantification of vacuoles displaying normal (even distribution) and abnormal SAG1 signal (uneven, patchy distribution with predominant accumulation inside the residual body), based on IFA images as shown in panel A. **C)** IFAs, showing staining of the rhoptry marker ARO and actin in TIR1 and GNA-mAID-Ty parasites after varying durations of auxin (IAA) treatment. **D)** Quantification of vacuoles displaying normal (club-shaped) and abnormal rhoptry morphology (shorter rhoptries with diffuse staining), based on IFA images as shown in panel C. **E)** Relative glycoinositolphospholipid (GIPL) abundance of untreated (–IAA) or IAA-treated (+IAA, 36 h) TIR1 and GNA1-mAID-Ty parasites. **F)** Percent of invaded TIR1 and GNA1-mAID-Ty parasite in the absence (–IAA) or after IAA treatment (18 hours) as determined by a red/green invasion assay. **G)** Quantification of glycoinositolphospholipids (GIPLs) in cells grown with the indicated treatments/supplementations for 18 hours. **H)** Percentage of invaded TIR1 and GNA1-mAID-Ty parasites, following the indicated treatment over 18 hours. A) and C) show representative images of three independent experiments. B, D-H show the means and standard deviation (error bars) from one of three independent biological replicates, averaging technical triplicates. For B and D, >100 vacuoles were counted and categorised, per replicate. p-values are given in B, D-H following two-sided Student's t-tests, comparing the indicated conditions. p-values <0.05 were considered significant. Abbreviations: ARO, Armadillo repeats only protein. For other abbreviations, see Figs 3 and 4.

https://doi.org/10.1371/journal.ppat.1011979.g005

rescue of the intracellular growth rate (Fig 4E), GPI/ GIPL abundance (Fig 5G) and the parasites' ability to invade host cells (Fig 5H). In summary, GNA1 is critical for *T. gondii* replication and invasion and cannot be bypassed by GlcNAc salvage.

Discussion

The amino sugar pathway, also known as the hexosamine biosynthetic pathway, plays a crucial role in various organisms, including the apicomplexan parasite *P. falciparum* [20,21]. A critical function of the pathway in the related apicomplexan *T. gondii* is consistent with the highly negative fitness scores for most of the enzymes in the pathway, as reported by a genome-wide CRISPR sgRNA-based fitness screen [23]. However, the screen assigned a positive fitness score to GNA1, which catalyses the acetylation of GlcN6P to GlcNAc6P, contrasting with the assumed key function of this enzyme in the pathway. Our presented data reveal that the enzymatic activity of GNA1 in *T. gondii*, which was previously illustrated by *in vitro* activity assays [20], is critical for *T. gondii* tachyzoite replication and development. The discrepancy between our findings and the genome-wide fitness screen likely arises from an omission in the gene annotation, which failed to highlight the existence of several short GNA1 isoforms. Our data suggest that full size GNA1 (consistent with the annotated sequence [25]) is synthesised alongside several shorter isoforms. These shorter isoforms contain the critical acetyltransferase domain [44], and remain unaffected by several individual sgRNAs employed in the genome-wide fitness screen to disrupt GNA1 [23]. To our knowledge, most eukaryotic organisms exhibit only a single GNA1 isoform [45]. However, within the apicomplexan GNA1 family, *T. gondii* GNA1 stands out due to its distinctive and elongated N-terminus [20]. The function of this extended N-term remains unknown. Despite the valuable information provided by genome wide studies, our findings highlight the limitations of such approaches and automatic gene annotation, reinforcing the importance of studying genes individually for a thorough comprehension of their significance.

UDP-GlcNAc and UDP-GalNAc are the final products of the aminosugar synthesis pathway with UDP-GalNAc derived from UDP-GlcNAc through the activity of GalE epimerase [7]. UDP-GlcNAc is key for the synthesis of GPI anchors and free GIPLs, which are present on the surface of all *T. gondii* life stages [46–48]. SAG1, the primary surface antigen of *T. gondii*, is a GPI anchored protein crucial for host cell binding and invasion [49]. Consequently GPI anchors and GIPLs contribute to parasite virulence [50] and are essential for *T. gondii* survival [16]. Our results reveal that GNA1 depletion leads to a marked drop in GPI anchors, altering the localization of SAG1 and causing aberrant rhoptry morphology, severely impacting host cell invasion and intracellular growth. Furthermore, UDP-GlcNAc, along with other sugar nucleotides, plays a crucial role in the biosynthesis of *N*-glycans, modifying numerous proteins in the *T. gondii* secretory pathway [7]. Several studies suggest that *N*-glycosylation is essential for parasite invasion, motility, and viability [8,23,51]. Indeed, *N*-glycosylation, but also GPI anchor biosynthesis and the amino sugar metabolism are among the metabolic pathways with the highest proportion of fitness-conferring genes in *T. gondii* tachyzoites, as reported by a recent study [22]. In summary, our data emphasize the importance of GNA1 for the amino sugar pathway and UDP-GlcNAc synthesis, highlighting the pivotal role of this metabolic route for parasite virulence and survival.

Depletion of GNA1 results in the accumulation of GlcN6P, and the reduction or absence of the downstream metabolites GlcNAc6P, GlcNAc1P and UDP-GlcNAc. While growth can be rescued by supplementing the media with high concentrations of GlcNAc in *P. falciparum* and other organisms [21,34,35], GlcNAc supplementation fails to rescue the lack of GNA1 in *T. gondii*. GlcN supplementation also proved ineffective in recovering parasite growth. Despite

the inability to rescue parasite growth, the absence of Glc in the media enhances GlcNAc salvaging, replenishing UDP-GlcNAc levels. This strongly suggests a competition between Glc and GlcNAc at the uptake or phosphorylation processes. Nevertheless, the recovery of GPI anchors /GIPLs and parasite growth through GlcNAc salvage is only partial when Glc is absent. The low levels of Fru6P indicate incomplete gluconeogenesis via glutamine, the predominant carbon source for *T*. *gondii* in absence of Glc [47]. In addition, these scant amounts of Fru6P in GlcNAc-supplemented TIR1 parasites under Glc depletion, strongly suggest the lack of an amino sugar catabolic pathway in *T*. *gondii*. Notably, the pronounced accumulation of GlcN6P observed in *T*. *gondii* GNA1 mutants could also contribute to the limited rescue observed with GlcNAc supplementation, by hindering an unidentified pathway and/or by depleting ATP [52,53]. Intriguingly, the accumulation of GlcN6P correlated more closely with a drop in GPI/ GIPL levels and concomitant impairment of parasite invasion than UDP-GlcNAc levels, indicating a potentially toxic impact of this surge in GlcN6P. Indeed, glucosamine has been shown to interfere with *P*. *falciparum* asexual intraerythrocytic growth at high doses [54–56]. Specifically, glucosamine was proposed to inhibit acylation of the GPI anchor in *P*. *falciparum* [54] and was also shown to inhibit the *N*-glycosylation of influenza virus haemagglutinin via an unknown mechanism [57]. Similar inhibitory mechanisms could be occurring in *T*. *gondii* following the accumulation of GlcN6P. However, the notable upsurge of the GlcN6P pool is most probably well above levels which could be obtained through a pharmacological inhibition of GNA1. Likewise, the high concentration of GlcNAc needed for partial *T*. *gondii* growth recovery remains far from physiological levels [58], suggesting that the likelihood of rescuing GNA1-depleted parasites under physiological conditions is very remote. In summary, the incomplete rescue in GlcNAc supplemented media strongly suggests the inability of a metabolic bypass to overcome GNA1 deficiency. This spotlights *T*. *gondii* GNA1 as a potential drug target to tackle toxoplasmosis.

T. *gondii* GNA1 belongs to a specific gene family, with an independent evolutionary origin within the phylum Apicomplexa [20]. Apicomplexan GNA1s exhibit distinct features and conserved motifs, and a recent structural study highlighted the divergent binding sites for GlcN6P and acetyl-CoA in *Cryptosporidium parvum* GNA1 compared to human GNA1, including important variations in key residues [21]. The key role of the amino sugar pathway for *T*. *gondii* viability, and the predicted significance of GPI anchors and GlcNAc-containing glycoconjugates across *T*. *gondii*'s life cycle [7,22], underscore the potential of GNA1 as a versatile multistage therapeutic target in toxoplasmosis that could be exploited for selective parasite inhibition.

Current drug therapies for human toxoplasmosis lack specificity, often leading to adverse effects and inconsistent efficacy [5,59]. Novel treatments against *T*. *gondii* must target the slow growing bradyzoites [60] to eradicate the chronic stage, which poses a threat to infected immunocompromised individuals [61]. Targeting bradyzoites efficiently is hindered by several hurdles: drugs must cross the blood-brain barrier and traverse the cyst wall and must act on enzymes/pathways that are critical for the poorly characterized metabolism of bradyzoites [62]. Intriguingly, the cyst in which bradyzoites reside and persist is heavily glycosylated, containing high levels of GlcNAc and GalNac residues [63]. A previous study highlighted that glycosylation of the cyst wall is critical for *T*. *gondii* persistence [17]. Specifically, Caffaro *et al*., demonstrated that the nucleotide sugar transporter *Tg*NST1 is required for cyst wall glycosylation and its disruption impairs the ability of *T*. *gondii* to persist but is dispensable for tachyzoites *in vitro* and during acute infection *in vivo* [17]. We demonstrate here that GNA1 is highly fitness-conferring for tachyzoites and can be expected to be essential for bradyzoites given the high need for UDP-GlcNAc and UDP-GalNAc during persistence [17], making it a promising candidate for a drug target.

Material and methods

Parasite lines, culture and treatments

Parasites stably expressing TIR1 were a generous gift from the laboratory of David Sibley [29]. These were maintained by regular passages in human foreskin fibroblasts (HFF-1, ATCC SCRC-1041), in Dulbecco Modified Eagle Medium (DMEM, Gibco, 41966–029) supplemented with foetal bovine serum (FBS, Gibco, 10270–106, 5% v/v), L-glutamine (Gibco, 20530–024, additional 2 mM) and Gentamycin (Gibco, 15750–045, 25 μg/ml), incubated in humidified incubators at 37˚C and 5% CO_2.

Auxin (IAA, Sigma-Aldrich, I-2886) was added to cultures at 500 μM final in ethanol as indicated for each experiment. Supplementations with sugars (Glc–Agilent, 103577, GlcN–Sigma-Aldrich, G1514 or GlcNAc–Sigma-Aldrich, A3286) were performed as described for each experiment in regular medium, as above or in DMEM without Glc (Gibco, 11966–025) supplemented with 5% (v/v) dialysed FBS (Pan Biotech P30-2102; 10,000 Da exclusion size membrane) and 10 mM L-glutamine (Agilent, 103579), in addition to the 2 mM L-glutamine present in DMEM and the supplemented 2 mM L-glutamine (see above).

Generation of transgenic parasites

The GNA1-mAID-Ty parasite line was generated through co-transfection of a CRISPR-Cas9 expression plasmid [27] with a guide RNA (P1, S1 Table) targeting the 3'-UTR of GNA1 (TTGT1_243600) and a homology repair template encoding the mAID domain, the 3-Ty domain and the *hxgprt* resistance cassette, amplified with the primers P2 and P3 (S1 Table) by KOD PCR (Sigma-Aldrich, KOD DNA Polymerase, from *Pyrococcus sp*. Strain KOD1). Transfected parasites were selected in medium containing mycophenolic acid (25 μg/ml) and xanthine (50 μg/ml) over one week and cloned by serial dilution followed by a second round of cloning. Subclones were frozen and a single clone was used in the following experiments.

Correct integration of the homology template at the desired location was assessed by PCR (GoTaq DNA Polymerase, Promega) on extracted genomic DNA (Promega Wizard DNA Extraction) testing three amplifications using primers P4 and P5, P4 and P6 and P4 and P7 amplifying under the following conditions: 95˚C, 2 min; (95˚C, 15 s; 57˚C 15 s; 72˚C 1.5 min) × 35; 72˚C, 5 min on a SimpliAmp Thermal Cycler (Applied Biosystems).

Immunofluorescence assays

Confluent monolayer of HFF cells grown on coverslips were inoculated with 10 μl of freshly egressed parasite cultures and treated with IAA as or other supplementations as indicated for each experiment. Twenty-four hours after inoculation, parasites were fixed with 4% PFA and 0.05% glutaraldehyde for 10 min, before quenching with 0.1 M glycine in phosphate-buffered saline (PBS) for 20 min. Infected host cells were permeabilized using 0.2% Triton X-100/PBS for 20 min, followed by 20 min incubation in (2% BSA/0.2% Triton X-100/PBS to block unspecific binding and subsequently probed with different primary antibodies diluted in 2% BSA/0.2% Triton X-100/PBS for 1 hour. The following primary antibodies were used as indicated for each experiment: α-Ty (1:10, mouse monoclonal, BB2), α-SAG1 (1:10, mouse, T4-1E5), polyclonal rabbit α-GAP45 (1:10,000, used for growth assay) [64], monoclonal mouse α-actin (1:20) [65], polyclonal rabbit α-CPN60 [66] and mouse monoclonal α-5F4 (F1 ATPase beta subunit, P. Bradley), polyclonal rabbit α-ARO [40]. The probed monolayer was washed (3 × 5 min, 0.2% Triton X-100/PBS) and probed with a secondary antibody: anti mouse Alexa fluor 488 (Invitrogen, A11001), anti-rabbit Alexa fluor 594 (Invitrogen, A11012). Following three washing steps as above, the coverslips were mounted on microscopy slides using DAPI-

containing FluoromountG (SouthernBiotech). Slides were viewed on an Eclipse Ti inverted microscope (Nikon). For growth assays, the number of parasites was counted in >100 vacuoles per condition for three independent biological replicates. Images were acquired using an LSM 700 confocal scanning microscope (Zeiss) and images were processed using Fiji Image J software.

Western blots

Parasites were harvested from a freshly lysed dish, washed with PBS, and resuspended in SDS–PAGE buffer (50 mM Tris-HCl, pH 6.8, 10% glycerol, 2 mM EDTA, 2% SDS, 0.05% bromophenol blue, and 100 mM dithiothreitol (DTT)). Following boiling for 10 min, samples were subjected to SDS–PAGE under reducing conditions. Proteins were transferred to a hybond ECL nitrocellulose membrane using a wet transfer system (Bio-Rad Laboratories, Hercules, CA, USA). The membrane was incubated in α-Ty antibody (1:10, mouse monoclonal, BB2) and rabbit α-catalase as a loading control [67], diluted in PBS, 0.05% Tween20, 5% skimmed milk. Following three washing steps, the membrane was incubated with the secondary antibodies (goat α-mouse, horse radish peroxidase conjugated, Sigma-Aldrich, A5278). Signal was visualized using the SuperSignal West Pico PLUS Chemiluminescent Substrate (ThermoFisher Scientific, 34580). Images were taken using the Bio-Rad ChemiDoc MP Imaging System and images were processed using Bio-Rad Image Lab software.

Plaque assays

Serial dilutions of parasite cultures were incubated on a confluent host cells monolayer in 12- or 24-well plates for 7 days. Afterwards, the infected monolayer was washed with PBS and fixed with 4% paraformaldehyde (PFA) for 10 min. Host cells were stained with a crystal violet solution (12.5 g crystal violet, 125 ml ethanol mixed with 500 ml water containing 1% (*w/v*) ammonium oxalate) over three hours. Wells were washed three times with deionized water to remove excess crystal violet and images of dried wells recorded.

Invasion (red/green) assays

Parasites from a freshly egressed culture treated as described for each experiment were diluted 1:10 and 150 μl of parasite solution used to infect a coverslip with confluent HFFs in a 24-well plate. The plate was gently spun for 1 min at 1,100 *g* and subsequently incubated in a water bath at 37˚C. Cells were fixed with 4% PFA and 0.05% glutaraldehyde for 7 min, before quenching with 0.1 M glycine in PBS for 10 min. Unspecific binding was blocked with (2% BSA in PBS–without triton), followed by incubation with α-SAG1 (1:10, mouse, T4-1E5) as above but without triton. Wells were washed three times with PBS before fixing cells with 4% PFA for 7 min. The next steps, permeabilization, blocking, primary antibody incubation, washing, secondary antibody incubation, washing and mounting were carried out as described above for the IFA. Polyclonal rabbit α-GAP45 (1:10,000) [64] was used as primary antibody and SAG1 and GAP45 were revealed in green and red, respectively, using the secondary antibodies as above for the IFA. Slides were viewed on an Eclipse Ti inverted microscope (Nikon). More than 100 parasites were counted per biological triplicate and categorised as invaded (red staining only) or non-invaded (red and green staining).

Stable isotope labelling of extracellular parasites

Pellets of filter-purified parasites (see below) were resuspended in 2 ml of DMEM without Glc (Gibco, 11966–025) supplemented with 5% (v/v) dialysed FBS (Pan Biotech P30-2102; 10,000

Da exclusion size membrane) and 10 mM U-$^{13}C_6$-Glc (Cambridge Isotope Laboratories, CLM-1396) or U-$^{13}C_6$-glucosamine (Cambridge Isotope Laboratories, CLM-9883) or U-$^{13}C_6$-*N*-acetylglucosamine (Cambridge Isotope Laboratories, CLM-1827) and incubated in a conical tube for five hours in humidified incubators at 37˚C and 5% CO_2 prior to addition of excess ice-cold PBS, centrifugation and PBS washes as described above. Samples were agitated intermittently to facilitate gas exchange.

Harvest of parasites for mass spectrometry analyses

Freshly egressing or intracellular parasites were harvested as follows: medium was aspirated, and the metabolism quenched through addition of ice-cold PBS. The monolayer was scraped, and parasites released via multiple passages through a 26G needle. The parasite solution was passed through a filter of 3 μm exclusion size (Merck-Millipore, TSTP04700) to remove host cell debris and collected in 15 ml conical tubes. Parasites were pelleted (2000 *g*, 4˚C, 25 min) and washed two more times with ice-cold PBS. Residual PBS was removed, and pellets of 10^8 parasites resuspended in medium as indicated below for labelling of extracellular parasites or stored at −80˚C until metabolite extraction. Samples were treated identically and swiftly to assure reproducible results.

Sample preparation for GC-MS analyses

Metabolite extraction was performed as previously described but without a heating step [68]. In brief, parasite pellets were placed on ice for five min before addition of 50 μl chloroform followed by 200 μl methanol:ultrapure water (3:1, including scyllo inositol as an internal standard, 1 nmol, Sigma-Aldrich, I8132). Extraction was facilitated through vigorous vortexing. Samples were spun (20,000 *g*, 4˚C, 10 min) and the supernatant transferred to a new vial containing 100 μl ice-cold ultrapure water. Samples were vortexed and spun (20,000 *g*, 4˚C, 10 min). The lower, organic phase (apolar, 50 μl) and the upper, polar phase (300 μl) were processed further as outlined below.

Sample preparation for LC-MS analyses

Cells were harvested and washed as described above. Pellets were reconstituted in 60 μl acetonitrile:ultrapure water (4:1, containing $^{13}C_6$/^{15}N-isoleucine as internal standard, 40 μM, Cambridge Isotope Laboratories, CNLM-561-H) and vortexed vigorously. Extracts were spun (20,000 *g*, 4˚C, 10 min) and the clear supernatant transferred to a mass spectrometry vial with insert. The metabolite extraction is based on that described in previous studies [69].

GIPL quantification via GC-MS (crude lipid extract)

GIPL quantification analysis and quantification was performed via methanolysis as previously described [41,70]. The apolar phase was transferred to a flame-sealed glass tube (Sigma-Aldrich, Z328510) and dried in a centrifugal evaporator. Next, 50 μl methanolic hydrochloric acid (HCl, Supelco, 33354) were added, the tube flame-sealed under vacuum and incubated in an oven at 80˚C over night. The next day, the glass tube was opened, and the content transferred to a mass spectrometry vial insert containing 10 μl pyridine to neutralise the pH. The solution was dried in a centrifugal evaporator and further derivatised through addition of 20 μl pyridine and 20 μl N, O-Bis(trimethylsilyl) trifluoracetamid 99% (Supelco, B-023). Samples were analysed on an 8890 GC System (Agilent) equipped with a DB5 capillary column (J&W Scientific, 30 m, 250 μm inner diameter, 0.25-μm film thickness), with a 10-m inert duraguard, connected to a 5977B GC/MSD in electron impact (EI) mode equipped with 7693A

autosampler (Agilent). The GC-MS settings were as follows: Inlet temperature: 270˚C, MS transfer line temperature: 280˚C, MS source temperature: 230˚C and MS quadrupole temperature: 150˚C. The oven gradient during the sample run was as follows: 80˚C (2 min); 80˚C to 140˚C at 30˚C/min; 140˚C to 250˚C at 5˚C/min; 250˚C to 310˚C at 15˚C/min; 310˚C for 2 min. Man and FA C16:0 derivatives were identified based on the ion spectra and retention times of authentic standards. Final analyses were performed in selected ion monitoring (SIM) mode, detecting the ions *m/z* 204 (Man derivative) and *m/z* 270 (FA C16:0 methyl ester), following injection of 1 μl in split mode (1:50). The signal obtained for Man was normalised to that of the FA C16:0 methyl ester in the same sample and GIPL levels were expressed as relative abundances relative to the control (TIR1 −IAA, abundance = 1). Data were analysed using MassHunter (Quantitative Analysis and Qualitative Analysis 10.0, Agilent) and Excel (Microsoft).

GIPL quantification via butanol partitioning

GIPLs were extracted as previously described by Azzouz *et al.* [43] with few noteworthy differences: an additional step was included to wash the water-saturated butanol extract with butanol-saturated water to remove any possible free (non-lipid bound) sugar residues. Also, in contrast to the methodology described by Azzouz *et al.* [43], samples were dried in a centrifugal evaporator and no white precipitate was observed upon drying. In consequence, the entire dried extract was reconstituted in water-saturated butanol, transferred to a glass tube, and processed as described above for methanolysis. The GC-MS was operated as outlined above but in Scan mode (*m/z* 80–800). The signal intensity obtained for mannose (*m/z* 204) was normalised to that of different fatty acids (C16:1, *m/z* 268; C20:1, *m/z* 292) and myo-inositol (*m/z* 318) and expressed as relative abundances relative to the control (TIR1 −IAA, abundance = 1). Identity of these metabolites was assigned based on the ion spectra and retention times of authentic standards. Data were analysed using MassHunter (Quantitative Analysis and Qualitative Analysis 10.0, Agilent) and Excel (Microsoft).

Targeted Aminosugar Profiling via GC-MS

Polar metabolites were derivatised and analysed as previously described [68]. In brief, the polar phase was sequentially dried within a mass spectrometry insert in a centrifugal evaporator (50 μl at a time) and further dried and concentrated through addition of methanol. The dried metabolite extract was derivatised through addition of 20 μl pyridine containing methoxyamine hydrochloride at 20 mg/ml and incubation at room temperature overnight. The following day, 20 μl *N*, O-Bis(trimethylsilyl) trifluoracetamid 99% (Supelco, B-023) were added and samples vortexed and analysed by GC-MS. The injection volume and MS temperatures were as described above but using the following GC oven gradient: 70˚C (1 min); 70˚C to 295˚C at 12.5˚C/min; 295˚C to 320˚C at 25˚C/min; 320˚C for 2 min. The MS was operated in SIM mode, detecting the ions *m/z* 356, 357, 358 and 359 to determine labelling in the desired sugars (see S3 Fig), as well as *m/z* 318 (internal standard, scyllo inositol). The ^{13}C-fractional labelling was determined by measuring the isotopologue abundance for *m/z* 357, 358 and 359 and correcting for occurrence of natural isotopes [71]. Metabolites were identified based on the analysis of authentic standards (see S3 Fig). Data were analysed using MassHunter (Quantitative Analysis and Qualitative Analysis 10.0, Agilent) and Excel (Microsoft). Metabolite intensities were normalised to the internal standard (scyllo inositol) and expressed as relative abundances relative to the control (TIR1 −IAA, abundance = 1).

Targeted Aminosugar Profiling via LC-MS/MS

Sample analyses were performed on an Agilent LC-MS (Santa Clara, CA, USA) using MassHunter B.08.00 software for system control and data acquisition. 1290 Infinity LC comprised a binary pump, HiP autosampler, column oven, and Flexible Cube module. The LC was hyphenated to a 6490 triple-quadrupole detector through an Agilent Jet Stream ion source. HILIC chromatographic separation was conducted on a Waters Acquity Premier BEH Amide column (2.1 × 150 mm, 1.7 μm) kept at 35˚C, a longer version with PREMIER coating compared to the column used in the referenced study [72], for reduced adsorption and improved separation. Elution was performed at a flow rate of 0.4 ml min^{-1}, using the following gradient of mobile phases [72]: A (10 mM AF + 0.15% FA in MeCN:H_2O 85:15 v/v) and B (10 mM AF + 0.15% FA in H_2O): 0–6 min 0% B, 6.1 min 5.9% B, 10 min 17.6% B, 12 min 29.4% B and back to 0% B from 12 to 18 minutes for column re-equilibration. Samples were kept at 6˚C and injection volume was 7 μl. Ion source parameters were as follow: Jet Stream gas temperature and flow rate were 250˚C and 15 l min^{-1} respectively, while for sheath gas they were set to 400˚C and 11 l min^{-1}. Nebulizer pressure was 40 psi, and a 3000 V capillary voltage was used. Ion funnel high/low pressure radio-frequencies were set to 150/60 for positive ionization transitions and 90/60 for negative ones.

Multiple reaction monitoring transitions were optimized using Agilent MassHunter Optimizer B.08.00 using individual solutions of the compounds dissolved at 100 μM in 80% ACN. The metabolite standards used here to determine the retention time and optimize the transitions were: D-fructose-6-phosphate disodium salt (Sigma-Aldrich, F3627); D-glucosamine-6-phosphate (Sigma-Aldrich, G5509); *N*-acetyl-D-glucosamine-6-P sodium salt (Sigma-Aldrich, A4394), *N*-acetyl-D-glucosamine-1-P disodium salt (Sigma-Aldrich, A2142) Uridine 5'diphosphate-*N*-acetylglucosamine sodium salt (Sigma-Aldrich, U4375). Collision energy and cone voltage were optimized and at least three fragments derived from the $[M+H]^+$, $[M+Na]^+$ or $[M-H]^-$precursor ions were used to monitor each molecule. The specific transitions, MS source and ion funnel conditions can be found in S2 Table. Data were processed using Skyline 22.2. Peak identity was confirmed based on its qualifier transitions and retention time compared to those of standard compounds (RSD < 3%). The relative abundance of each molecule was expressed as the sum of all the areas of the corresponding transitions, normalized to the internal standard and expressed as relative abundance in relation to TIR1 −IAA abundance = 1, using Excel (Microsoft).

Supporting information

S1 Fig. GNA1 sequence, genome-wide fitness screen guides, locus modification and genomic PCR. A) GNA1 coding sequence as found on ToxoDB. The initial start codon is highlighted in green, the stop codon in red. Four additional 'in-frame' start codons were found and are also highlighted by green shading. Blue (guide with positive score) and red shading (guide with negative score; intensity of shading indicating score) highlights the sequence of single guide RNAs (sgRNA) used in the genome-wide fitness screen. For overlapping guides, the first guide is shown as underlined, the second guide is shown in bold. The name/number of the guides and their respective fitness score is provided. The listing is from left to right and from top to bottom in the order of their appearance in the coding sequence. Note that the first 4 guides only affect the longest putative GNA1 product, while the last 4 guides affect all GNA1 products, including the shortest potential GNA1 protein (highlighted in italic). The acetyltransferase domain, needed for the catalytic activity is highlighted in purple and bold. **B)** Schematic depiction of the GNA1 locus and its modification through insertion of a mini auxin inducible degron (mAID) domain, a 3-Ty tag and a *hxgprt* resistance cassette for selection. **C)** Schematic showing the binding sites of primers used to validate the successful modification of

the GNA1 locus and integration PCR, showing the expected bands following amplification with the indicated primers. Sequences of these primers are listed in S1 Table.
(TIF)

S2 Fig. GC-MS chromatograms ion spectra and structures of relevant metabolites. A) Authentic standards of glucose-6-phosphate (Glc6P) and *N*-acetylglucosamine-6-phosphate (GlcNAc6P) were derivatised via methoximation and silylatation. Their overlayed gas chromatography-mass spectrometry (GC-MS) chromatograms are shown. **B-C)** Structures of the derivatives and their ion spectra at the indicated retention times (see asterisk in A) are provided. Note that both derivatives share a common fragment of *m/z* 357, which contains 2 carbons of the sugar but both compounds also exhibit unique fragments, including the ions of *m/z* 706 and *m/z* 675, corresponding to the $[M\text{-}15]^+$ ions following loss of a methyl group from the Glc6P and GlcNAc6P derivatives, respectively. **D)** Representative selected ion monitoring (SIM) ion profile, showing traces of the ions *m/z* 357 and *m/z* 359 of an unlabelled parasite extract. The peaks corresponding to the Glc6P and GlcNAc6P derivatives are highlighted with an asterisk. **E, F)** Detail of the ion profiles shown in D for Glc6P and GlcNAc6P, respectively. **G)** Representative selected ion monitoring (SIM) ion profile, showing the traces of the ions *m/z* 357 and *m/z* 359 in an extract of parasites labelled during intracellular growth for 24 hours with 10 mM U-$^{13}C_6$-Glc. The peaks corresponding to the Glc6P and GlcNAc6P derivatives are highlighted with an asterisk. **H-I)** Detail of the ion profiles shown in G for Glc6P and GlcNAc6P, respectively. **J)** Representative ion spectrum (Scan, *m/z* 80–800) for the GlcNAc6P derivative from the same sample as shown in G-I. Note that the ion *m/z* 675 shifts to *m/z* 683, indicating that all carbons, including those of the acetyl group are labelled from the provided U-$^{13}C_6$-Glc.
(TIF)

S3 Fig. Representative LC-MS signals for the precursor and product ions of GlcN6P and UDP-GlcNAc. A) Signal obtained for GlcN6P precursor and product ions in parasites depleted in GNA1 for 18 hours (GNA1-mAID-Ty +IAA) and the relevant controls (TIR1 +IAA, GNA1-mAID-Ty–IAA) by LC-MS. **B)** Signal obtained for UDP-GlcNAc precursor and product ions in parasites depleted in GNA1 for 18 hours (GNA1-mAID-Ty +IAA) and the relevant controls (TIR1 +IAA, GNA1-mAID-Ty–IAA) by LC-MS. The retention times and transitions are listed in the panels and can also be found in S2 Table.
(TIF)

S4 Fig. Organelle morphology and GPI quantification validation. Immunofluorescence assays (IFAs) were performed after auxin (IAA) treatment for the indicated durations and after 24 hours of intracellular growth. Cells were stained with **A)** antibodies marking actin and the apicoplast (chaperonin 60, CPN60) or **B)** antibodies staining the pellicle (GAP45) and the mitochondrion (5F4). Intactness of the apicoplast and mitochondrion was determined in three technical replicates of a single experiment. Images shown are representative of these analyses. **C-E)** Glycoinositolphospholipid (GIPL) quantification was validated by employing a distinct extraction protocol based on butanol-partitioning and normalising the signal obtained for GIPL-derived mannose to different fatty acids (C16:1, C or C20:1, D) or myo-inositol (E).
(TIF)

S1 Table. Primers. Description and sequence of primers used in this study.
(XLSX)

S2 Table. Transitions, MS source and ion funnel conditions. Table with details pertaining to LC-MS analyses.
(XLSX)

Author Contributions

Conceptualization: María Pía Alberione, Dominique Soldati-Favre, Luis Izquierdo, Joachim Kloehn.

Data curation: María Pía Alberione, Víctor González-Ruiz, Olivier von Rohr, Joachim Kloehn.

Formal analysis: María Pía Alberione, Víctor González-Ruiz, Olivier von Rohr, Joachim Kloehn.

Funding acquisition: Serge Rudaz, Dominique Soldati-Favre, Luis Izquierdo, Joachim Kloehn.

Investigation: María Pía Alberione, Víctor González-Ruiz, Olivier von Rohr, Joachim Kloehn.

Methodology: Víctor González-Ruiz, Joachim Kloehn.

Project administration: Serge Rudaz, Dominique Soldati-Favre, Luis Izquierdo, Joachim Kloehn.

Resources: Serge Rudaz, Dominique Soldati-Favre, Luis Izquierdo, Joachim Kloehn.

Supervision: Serge Rudaz, Dominique Soldati-Favre, Luis Izquierdo, Joachim Kloehn.

Validation: María Pía Alberione, Víctor González-Ruiz, Olivier von Rohr, Joachim Kloehn.

Visualization: María Pía Alberione, Dominique Soldati-Favre, Luis Izquierdo, Joachim Kloehn.

Writing – original draft: María Pía Alberione, Dominique Soldati-Favre, Luis Izquierdo, Joachim Kloehn.

Writing – review & editing: María Pía Alberione, Víctor González-Ruiz, Olivier von Rohr, Serge Rudaz, Dominique Soldati-Favre, Luis Izquierdo, Joachim Kloehn.

References

1. Nissapatorn V. *Toxoplasma gondii* and HIV: a never-ending story. Lancet HIV. 2017; 4(4):e146–e7. Epub 2017/02/06. https://doi.org/10.1016/S2352-3018(17)30003-6 PMID: 28159547.
2. Wang ZD, Wang SC, Liu HH, Ma HY, Li ZY, Wei F, et al. Prevalence and burden of *Toxoplasma gondii* infection in HIV-infected people: a systematic review and meta-analysis. Lancet HIV. 2017; 4(4):e177–e88. Epub 2017/02/06. https://doi.org/10.1016/S2352-3018(17)30005-X PMID: 28159548.
3. McAuley JB. Congenital Toxoplasmosis. J Pediatric Infect Dis Soc. 2014;3 Suppl 1(Suppl 1):S30–5. Epub 2014/09/19. https://doi.org/10.1093/jpids/piu077 PMID: 25232475; PubMed Central PMCID: PMC4164182.
4. Montoya JG, Liesenfeld O. Toxoplasmosis. Lancet. 2004; 363(9425):1965–76. Epub 2004/06/15. https://doi.org/10.1016/S0140-6736(04)16412-X PMID: 15194258.
5. Konstantinovic N, Guegan H, Stajner T, Belaz S, Robert-Gangneux F. Treatment of toxoplasmosis: Current options and future perspectives. Food Waterborne Parasitol. 2019; 15:e00036. Epub 2020/02/26. https://doi.org/10.1016/j.fawpar.2019.e00036 PMID: 32095610; PubMed Central PMCID: PMC7033996.
6. Weiss LM, Kim K. The development and biology of bradyzoites of *Toxoplasma gondii*. Front Biosci. 2000; 5:D391–405. Epub 2000/04/14. https://doi.org/10.2741/weiss PMID: 10762601; PubMed Central PMCID: PMC3109641.
7. Gas-Pascual E, Ichikawa HT, Sheikh MO, Serji MI, Deng B, Mandalasi M, et al. CRISPR/Cas9 and glycomics tools for *Toxoplasma* glycobiology. J Biol Chem. 2019; 294(4):1104–25. Epub 2018/11/23. https://doi.org/10.1074/jbc.RA118.006072 PMID: 30463938; PubMed Central PMCID: PMC6349120.
8. Luk FC, Johnson TM, Beckers CJ. N-linked glycosylation of proteins in the protozoan parasite *Toxoplasma gondii*. Mol Biochem Parasitol. 2008; 157(2):169–78. Epub 2007/12/22. https://doi.org/10.1016/j.molbiopara.2007.10.012 PMID: 18096254; PubMed Central PMCID: PMC2258246.

9. Bandini G, Albuquerque-Wendt A, Hegermann J, Samuelson J, Routier FH. Protein O- and C-Glycosylation pathways in *Toxoplasma gondii* and *Plasmodium falciparum*. Parasitology. 2019; 146(14):1755–66. Epub 2019/02/19. https://doi.org/10.1017/S0031182019000040 PMID: 30773146; PubMed Central PMCID: PMC6939170.

10. Bandini G, Haserick JR, Motari E, Ouologuem DT, Lourido S, Roos DS, et al. O-fucosylated glycoproteins form assemblies in close proximity to the nuclear pore complexes of *Toxoplasma gondii*. Proc Natl Acad Sci U S A. 2016; 113(41):11567–72. Epub 2016/09/25. https://doi.org/10.1073/pnas.1613653113 PMID: 27663739; PubMed Central PMCID: PMC5068260.

11. Bandini G, Leon DR, Hoppe CM, Zhang Y, Agop-Nersesian C, Shears MJ, et al. O-Fucosylation of thrombospondin-like repeats is required for processing of microneme protein 2 and for efficient host cell invasion by *Toxoplasma gondii* tachyzoites. J Biol Chem. 2019; 294(6):1967–83. Epub 2018/12/13. https://doi.org/10.1074/jbc.RA118.005179 PMID: 30538131; PubMed Central PMCID: PMC6369279.

12. Perez-Cervera Y, Harichaux G, Schmidt J, Debierre-Grockiego F, Dehennaut V, Bieker U, et al. Direct evidence of O-GlcNAcylation in the apicomplexan *Toxoplasma gondii*: a biochemical and bioinformatic study. Amino Acids. 2011; 40(3):847–56. Epub 2010/07/28. https://doi.org/10.1007/s00726-010-0702-4 PMID: 20661758.

13. Stwora-Wojczyk MM, Dzierszinski F, Roos DS, Spitalnik SL, Wojczyk BS. Functional characterization of a novel *Toxoplasma gondii* glycosyltransferase: UDP-*N*-acetyl-D-galactosamine:polypeptide *N*-acetylgalactosaminyltransferase-T3. Arch Biochem Biophys. 2004; 426(2):231–40. Epub 2004/05/26. https://doi.org/10.1016/j.abb.2004.02.013 PMID: 15158673.

14. Albuquerque-Wendt A, Jacot D, Dos Santos Pacheco N, Seegers C, Zarnovican P, Buettner FFR, et al. C-Mannosylation of *Toxoplasma gondii* proteins promotes attachment to host cells and parasite virulence. J Biol Chem. 2020; 295(4):1066–76. Epub 2019/12/22. https://doi.org/10.1074/jbc.RA119.010590 PMID: 31862733; PubMed Central PMCID: PMC6983843.

15. Striepen B, Dubremetz JF, Schwarz RT. Glucosylation of glycosylphosphatidylinositol membrane anchors: identification of uridine diphosphate-glucose as the direct donor for side chain modification in *Toxoplasma gondii* using carbohydrate analogues. Biochemistry. 1999; 38(5):1478–87. Epub 1999/02/04. https://doi.org/10.1021/bi981884q PMID: 9931013.

16. Wichroski MJ, Ward GE. Biosynthesis of glycosylphosphatidylinositol is essential to the survival of the protozoan parasite *Toxoplasma gondii*. Eukaryot Cell. 2003; 2(5):1132–6. Epub 2003/10/14. https://doi.org/10.1128/EC.2.5.1132–1136.2003 PMID: 14555496; PubMed Central PMCID: PMC219362.

17. Caffaro CE, Koshy AA, Liu L, Zeiner GM, Hirschberg CB, Boothroyd JC. A nucleotide sugar transporter involved in glycosylation of the *Toxoplasma* tissue cyst wall is required for efficient persistence of bradyzoites. PLoS Pathog. 2013; 9(5):e1003331. Epub 2013/05/10. https://doi.org/10.1371/journal.ppat.1003331 PMID: 23658519; PubMed Central PMCID: PMC3642066.

18. Tomita T, Sugi T, Yakubu R, Tu V, Ma Y, Weiss LM. Making Home Sweet and Sturdy: *Toxoplasma gondii* ppGalNAc-Ts Glycosylate in Hierarchical Order and Confer Cyst Wall Rigidity. mBio. 2017; 8(1). Epub 2017/01/12. https://doi.org/10.1128/mBio.02048-16 PMID: 28074022; PubMed Central PMCID: PMC5225312.

19. Chasen NM, Asady B, Lemgruber L, Vommaro RC, Kissinger JC, Coppens I, et al. A Glycosylphosphatidylinositol-Anchored Carbonic Anhydrase-Related Protein of *Toxoplasma gondii* Is Important for Rhoptry Biogenesis and Virulence. mSphere. 2017; 2(3). Epub 2017/05/23. https://doi.org/10.1128/mSphere.00027-17 PMID: 28529974; PubMed Central PMCID: PMC5437132.

20. Cova M, Lopez-Gutierrez B, Artigas-Jeronimo S, Gonzalez-Diaz A, Bandini G, Maere S, et al. The Apicomplexa-specific glucosamine-6-phosphate *N*-acetyltransferase gene family encodes a key enzyme for glycoconjugate synthesis with potential as therapeutic target. Sci Rep. 2018; 8(1):4005. Epub 2018/03/07. https://doi.org/10.1038/s41598-018-22441-3 PMID: 29507322; PubMed Central PMCID: PMC5838249.

21. Chi J, Cova M, de Las Rivas M, Medina A, Borges RJ, Leivar P, et al. *Plasmodium falciparum* Apicomplexan-Specific Glucosamine-6-Phosphate N-Acetyltransferase Is Key for Amino Sugar Metabolism and Asexual Blood Stage Development. mBio. 2020;11(5). Epub 2020/10/22. https://doi.org/10.1128/mBio.02045-20 PMID: 33082260; PubMed Central PMCID: PMC7587441.

22. Krishnan A, Kloehn J, Lunghi M, Chiappino-Pepe A, Waldman BS, Nicolas D, et al. Functional and Computational Genomics Reveal Unprecedented Flexibility in Stage-Specific *Toxoplasma* Metabolism. Cell Host Microbe. 2020; 27(2):290–306 e11. Epub 2020/01/29. https://doi.org/10.1016/j.chom.2020.01.002 PMID: 31991093.

23. Sidik SM, Huet D, Ganesan SM, Huynh MH, Wang T, Nasamu AS, et al. A Genome-wide CRISPR Screen in *Toxoplasma* Identifies Essential Apicomplexan Genes. Cell. 2016; 166(6):1423–35 e12. Epub 2016/09/07. https://doi.org/10.1016/j.cell.2016.08.019 PMID: 27594426; PubMed Central PMCID: PMC5017925.

24. Mio T, Yamada-Okabe T, Arisawa M, Yamada-Okabe H. *Saccharomyces cerevisiae* GNA1, an essential gene encoding a novel acetyltransferase involved in UDP-*N*-acetylglucosamine synthesis. J Biol Chem. 1999; 274(1):424–9. Epub 1998/12/29. https://doi.org/10.1074/jbc.274.1.424 PMID: 9867860.

25. Gajria B, Bahl A, Brestelli J, Dommer J, Fischer S, Gao X, et al. ToxoDB: an integrated *Toxoplasma gondii* database resource. Nucleic Acids Res. 2008; 36(Database issue):D553–6. Epub 2007/11/16. https://doi.org/10.1093/nar/gkm981 PMID: 18003657; PubMed Central PMCID: PMC2238934.

26. Lee VV, Judd LM, Jex AR, Holt KE, Tonkin CJ, Ralph SA. Direct Nanopore Sequencing of mRNA Reveals Landscape of Transcript Isoforms in Apicomplexan Parasites. mSystems. 2021; 6(2). Epub 2021/03/11. https://doi.org/10.1128/mSystems.01081-20 PMID: 33688018; PubMed Central PMCID: PMC8561664.

27. Shen B, Brown KM, Lee TD, Sibley LD. Efficient gene disruption in diverse strains of *Toxoplasma gondii* using CRISPR/CAS9. mBio. 2014; 5(3):e01114–14. Epub 2014/05/16. https://doi.org/10.1128/mBio.01114-14 PMID: 24825012; PubMed Central PMCID: PMC4030483.

28. Brown KM, Long S, Sibley LD. *Plasma Membrane* Association by N-Acylation Governs PKG Function in Toxoplasma gondii. mBio. 2017; 8(3). Epub 2017/05/04. https://doi.org/10.1128/mBio.00375-17 PMID: 28465425; PubMed Central PMCID: PMC5414004.

29. Brown KM, Long S, Sibley LD. Conditional Knockdown of Proteins Using Auxin-inducible Degron (AID) Fusions in *Toxoplasma gondii*. Bio Protoc. 2018; 8(4). Epub 2018/04/13. https://doi.org/10.21769/BioProtoc.2728 PMID: 29644255; PubMed Central PMCID: PMC5890294.

30. Donald RG, Roos DS. Gene knock-outs and allelic replacements in *Toxoplasma gondii*: HXGPRT as a selectable marker for hit-and-run mutagenesis. Mol Biochem Parasitol. 1998; 91(2):295–305. Epub 1998/05/05. https://doi.org/10.1016/s0166-6851(97)00210-7 PMID: 9566522.

31. MacRae JI, Sheiner L, Nahid A, Tonkin C, Striepen B, McConville MJ. Mitochondrial metabolism of glucose and glutamine is required for intracellular growth of *Toxoplasma gondii*. Cell Host Microbe. 2012; 12(5):682–92. Epub 2012/11/20. https://doi.org/10.1016/j.chom.2012.09.013 PMID: 23159057; PubMed Central PMCID: PMC3990185.

32. Sugi T, Tu V, Ma Y, Tomita T, Weiss LM. *Toxoplasma gondii* Requires Glycogen Phosphorylase for Balancing Amylopectin Storage and for Efficient Production of Brain Cysts. mBio. 2017; 8(4). Epub 2017/08/31. https://doi.org/10.1128/mBio.01289-17 PMID: 28851850; PubMed Central PMCID: PMC5574715.

33. Lyu C, Yang X, Yang J, Hou L, Zhou Y, Zhao J, et al. Role of amylopectin synthesis in *Toxoplasma gondii* and its implication in vaccine development against toxoplasmosis. Open Biol. 2021; 11(6):200384. Epub 2021/06/16. https://doi.org/10.1098/rsob.200384 PMID: 34129780; PubMed Central PMCID: PMC8205521.

34. Boehmelt G, Wakeham A, Elia A, Sasaki T, Plyte S, Potter J, et al. Decreased UDP-GlcNAc levels abrogate proliferation control in EMeg32-deficient cells. EMBO J. 2000; 19(19):5092–104. Epub 2000/10/03. https://doi.org/10.1093/emboj/19.19.5092 PMID: 11013212; PubMed Central PMCID: PMC302091.

35. Lockhart DEA, Stanley M, Raimi OG, Robinson DA, Boldovjakova D, Squair DR, et al. Targeting a critical step in fungal hexosamine biosynthesis. J Biol Chem. 2020; 295(26):8678–91. Epub 2020/04/29. https://doi.org/10.1074/jbc.RA120.012985 PMID: 32341126; PubMed Central PMCID: PMC7324522.

36. Dzierszinski F, Mortuaire M, Cesbron-Delauw MF, Tomavo S. Targeted disruption of the glycosylphosphatidylinositol-anchored surface antigen SAG3 gene in *Toxoplasma gondii* decreases host cell adhesion and drastically reduces virulence in mice. Mol Microbiol. 2000; 37(3):574–82. Epub 2000/08/10. https://doi.org/10.1046/j.1365-2958.2000.02014.x PMID: 10931351.

37. Jacquet A, Coulon L, De Neve J, Daminet V, Haumont M, Garcia L, et al. The surface antigen SAG3 mediates the attachment of *Toxoplasma gondii* to cell-surface proteoglycans. Mol Biochem Parasitol. 2001; 116(1):35–44. Epub 2001/07/21. https://doi.org/10.1016/s0166-6851(01)00297-3 PMID: 11463464.

38. Binder EM, Lagal V, Kim K. The prodomain of *Toxoplasma gondii* GPI-anchored subtilase TgSUB1 mediates its targeting to micronemes. Traffic. 2008; 9(9):1485–96. Epub 2008/06/06. https://doi.org/10.1111/j.1600-0854.2008.00774.x PMID: 18532988; PubMed Central PMCID: PMC3556455.

39. Robinson SA, Smith JE, Millner PA. *Toxoplasma gondii* major surface antigen (SAG1): in vitro analysis of host cell binding. Parasitology. 2004;128(Pt 4):391–6. Epub 2004/05/21. https://doi.org/10.1017/s0031182003004736 PMID: 15151144.

40. Mueller C, Klages N, Jacot D, Santos JM, Cabrera A, Gilberger TW, et al. The *Toxoplasma* protein ARO mediates the apical positioning of rhoptry organelles, a prerequisite for host cell invasion. Cell Host Microbe. 2013; 13(3):289–301. Epub 2013/03/19. https://doi.org/10.1016/j.chom.2013.02.001 PMID: 23498954.

41. Blume M, Nitzsche R, Sternberg U, Gerlic M, Masters SL, Gupta N, et al. A *Toxoplasma gondii* Gluconeogenic Enzyme Contributes to Robust Central Carbon Metabolism and Is Essential for Replication

and Virulence. Cell Host Microbe. 2015; 18(2):210–20. Epub 2015/08/14. https://doi.org/10.1016/j.chom.2015.07.008 PMID: 26269956.

42. Kloehn J, Oppenheim RD, Siddiqui G, De Bock PJ, Kumar Dogga S, Coute Y, et al. Multi-omics analysis delineates the distinct functions of sub-cellular acetyl-CoA pools in *Toxoplasma gondii*. BMC Biol. 2020; 18(1):67. Epub 2020/06/18. https://doi.org/10.1186/s12915-020-00791-7 PMID: 32546260; PubMed Central PMCID: PMC7296777.

43. Azzouz N, Shams-Eldin H, Schwarz RT. Removal of phospholipid contaminants through precipitation of glycosylphosphatidylinositols. Anal Biochem. 2005; 343(1):152–8. Epub 2005/06/16. https://doi.org/10.1016/j.ab.2005.04.030 PMID: 15955525.

44. Dyda F, Klein DC, Hickman AB. GCN5-related *N*-acetyltransferases: a structural overview. Annu Rev Biophys Biomol Struct. 2000; 29:81–103. Epub 2000/08/15. https://doi.org/10.1146/annurev.biophys.29.1.81 PMID: 10940244; PubMed Central PMCID: PMC4782277.

45. Riegler H, Herter T, Grishkovskaya I, Lude A, Ryngajllo M, Bolger ME, et al. Crystal structure and functional characterization of a glucosamine-6-phosphate *N*-acetyltransferase from *Arabidopsis thaliana*. Biochem J. 2012; 443(2):427–37. Epub 2012/02/15. https://doi.org/10.1042/BJ20112071 PMID: 22329777.

46. Azzouz N, Shams-Eldin H, Niehus S, Debierre-Grockiego F, Bieker U, Schmidt J, et al. *Toxoplasma gondii* grown in human cells uses GalNAc-containing glycosylphosphatidylinositol precursors to anchor surface antigens while the immunogenic Glc-GalNAc-containing precursors remain free at the parasite cell surface. Int J Biochem Cell Biol. 2006; 38(11):1914–25. Epub 2006/07/11. https://doi.org/10.1016/j.biocel.2006.05.006 PMID: 16822699.

47. Boothroyd JC, Hehl A, Knoll LJ, Manger ID. The surface of *Toxoplasma*: more and less. Int J Parasitol. 1998; 28(1):3–9. Epub 1998/03/21. https://doi.org/10.1016/s0020-7519(97)00182-3 PMID: 9504330.

48. Manger ID, Hehl AB, Boothroyd JC. The surface of *Toxoplasma* tachyzoites is dominated by a family of glycosylphosphatidylinositol-anchored antigens related to SAG1. Infect Immun. 1998; 66(5):2237–44. Epub 1998/05/09. https://doi.org/10.1128/IAI.66.5.2237–2244.1998 PMID: 9573113; PubMed Central PMCID: PMC108187.

49. Lekutis C, Ferguson DJ, Grigg ME, Camps M, Boothroyd JC. Surface antigens of *Toxoplasma gondii*: variations on a theme. Int J Parasitol. 2001; 31(12):1285–92. Epub 2001/09/22. https://doi.org/10.1016/s0020-7519(01)00261-2 PMID: 11566296.

50. Niehus S, Smith TK, Azzouz N, Campos MA, Dubremetz JF, Gazzinelli RT, et al. Virulent and avirulent strains of *Toxoplasma gondii* which differ in their glycosylphosphatidylinositol content induce similar biological functions in macrophages. PLoS One. 2014; 9(1):e85386. Epub 2014/02/04. https://doi.org/10.1371/journal.pone.0085386 PMID: 24489660; PubMed Central PMCID: PMC3904843.

51. Fauquenoy S, Hovasse A, Sloves PJ, Morelle W, Dilezitoko Alayi T, Slomianny C, et al. Unusual N-glycan structures required for trafficking *Toxoplasma gondii* GAP50 to the inner membrane complex regulate host cell entry through parasite motility. Mol Cell Proteomics. 2011; 10(9):M111 008953. Epub 2011/05/26. https://doi.org/10.1074/mcp.M111.008953 PMID: 21610105; PubMed Central PMCID: PMC3186202.

52. Marshall S, Nadeau O, Yamasaki K. Dynamic actions of glucose and glucosamine on hexosamine biosynthesis in isolated adipocytes: differential effects on glucosamine 6-phosphate, UDP-*N*-acetylglucosamine, and ATP levels. J Biol Chem. 2004; 279(34):35313–9. Epub 2004/06/17. https://doi.org/10.1074/jbc.M404133200 PMID: 15199059.

53. Plagemann PG, Erbe J. Transport and metabolism of glucosamine by cultured Novikoff rat hepatoma cells and effects on nucleotide pools. Cancer Res. 1973; 33(3):482–92. Epub 1973/03/01. PMID: 4347714.

54. Naik RS, Krishnegowda G, Gowda DC. Glucosamine inhibits inositol acylation of the glycosylphosphatidylinositol anchors in intraerythrocytic *Plasmodium falciparum*. J Biol Chem. 2003; 278(3):2036–42. Epub 2002/11/07. https://doi.org/10.1074/jbc.M208976200 PMID: 12419814.

55. Prommana P, Uthaipibull C, Wongsombat C, Kamchonwongpaisan S, Yuthavong Y, Knuepfer E, et al. Inducible knockdown of *Plasmodium* gene expression using the glmS ribozyme. PLoS One. 2013; 8(8):e73783. Epub 2013/09/12. https://doi.org/10.1371/journal.pone.0073783 PMID: 24023691; PubMed Central PMCID: PMC3758297.

56. Weiss MM, Oppenheim JD, Vanderberg JP. *Plasmodium falciparum*: assay in vitro for inhibitors of merozoite penetration of erythrocytes. Exp Parasitol. 1981; 51(3):400–7. Epub 1981/06/01. https://doi.org/10.1016/0014-4894(81)90127-2 PMID: 7014239.

57. Schwarz RT, Klenk HD. Inhibition of glycosylation of the influenza virus hemagglutinin. J Virol. 1974; 14(5):1023–34. Epub 1974/11/01. https://doi.org/10.1128/JVI.14.5.1023-1034.1974 PMID: 4473565; PubMed Central PMCID: PMC355615.

58. Wishart DS, Guo A, Oler E, Wang F, Anjum A, Peters H, et al. HMDB 5.0: the Human Metabolome Database for 2022. Nucleic Acids Res. 2022; 50(D1):D622–D31. Epub 2022/01/07. https://doi.org/10.1093/nar/gkab1062 PMID: 34986597; PubMed Central PMCID: PMC8728138.

59. Dunay IR, Gajurel K, Dhakal R, Liesenfeld O, Montoya JG. Treatment of Toxoplasmosis: Historical Perspective, Animal Models, and Current Clinical Practice. Clin Microbiol Rev. 2018; 31(4). Epub 2018/09/14. https://doi.org/10.1128/CMR.00057-17 PMID: 30209035; PubMed Central PMCID: PMC6148195.

60. Alday PH, Doggett JS. Drugs in development for toxoplasmosis: advances, challenges, and current status. Drug Des Devel Ther. 2017; 11:273–93. Epub 2017/02/10. https://doi.org/10.2147/DDDT.S60973 PMID: 28182168; PubMed Central PMCID: PMC5279849.

61. Murata Y, Sugi T, Weiss LM, Kato K. Identification of compounds that suppress *Toxoplasma gondii* tachyzoites and bradyzoites. PLoS One. 2017; 12(6):e0178203. Epub 2017/06/14. https://doi.org/10.1371/journal.pone.0178203 PMID: 28609444; PubMed Central PMCID: PMC5469451.

62. Christiansen C, Maus D, Hoppenz E, Murillo-Leon M, Hoffmann T, Scholz J, et al. In vitro maturation of *Toxoplasma gondii* bradyzoites in human myotubes and their metabolomic characterization. Nat Commun. 2022; 13(1):1168. Epub 2022/03/06. https://doi.org/10.1038/s41467-022-28730-w PMID: 35246532; PubMed Central PMCID: PMC8897399.

63. Boothroyd JC, Black M, Bonnefoy S, Hehl A, Knoll LJ, Manger ID, et al. Genetic and biochemical analysis of development in *Toxoplasma gondii*. Philos Trans R Soc Lond B Biol Sci. 1997; 352(1359):1347–54. Epub 1997/11/14. https://doi.org/10.1098/rstb.1997.0119 PMID: 9355126; PubMed Central PMCID: PMC1692023.

64. Plattner F, Yarovinsky F, Romero S, Didry D, Carlier MF, Sher A, et al. *Toxoplasma profilin* is essential for host cell invasion and TLR11-dependent induction of an interleukin-12 response. Cell Host Microbe. 2008; 3(2):77–87. Epub 2008/03/04. https://doi.org/10.1016/j.chom.2008.01.001 PMID: 18312842.

65. Herm-Gotz A, Weiss S, Stratmann R, Fujita-Becker S, Ruff C, Meyhofer E, et al. *Toxoplasma gondii* myosin A and its light chain: a fast, single-headed, plus-end-directed motor. EMBO J. 2002; 21(9):2149–58. Epub 2002/05/01. https://doi.org/10.1093/emboj/21.9.2149 PMID: 11980712; PubMed Central PMCID: PMC125985.

66. Agrawal S, van Dooren GG, Beatty WL, Striepen B. Genetic evidence that an endosymbiont-derived endoplasmic reticulum-associated protein degradation (ERAD) system functions in import of apicoplast proteins. J Biol Chem. 2009; 284(48):33683–91. Epub 2009/10/08. https://doi.org/10.1074/jbc.M109.044024 PMID: 19808683; PubMed Central PMCID: PMC2785210.

67. Ding M, Clayton C, Soldati D. *Toxoplasma gondii* catalase: are there peroxisomes in toxoplasma? J Cell Sci. 2000;113 (Pt 13):2409–19. Epub 2000/06/15. https://doi.org/10.1242/jcs.113.13.2409 PMID: 10852820.

68. Saunders EC, Ng WW, Chambers JM, Ng M, Naderer T, Kromer JO, et al. Isotopomer profiling of *Leishmania mexicana* promastigotes reveals important roles for succinate fermentation and aspartate uptake in tricarboxylic acid cycle (TCA) anaplerosis, glutamate synthesis, and growth. J Biol Chem. 2011; 286(31):27706–17. Epub 2011/06/04. https://doi.org/10.1074/jbc.M110.213553 PMID: 21636575; PubMed Central PMCID: PMC3149361.

69. Cobbold SA, M VT, Frasse P, McHugh E, Karnthaler M, Creek DJ, et al. Non-canonical metabolic pathways in the malaria parasite detected by isotope-tracing metabolomics. Mol Syst Biol. 2021; 17(4):e10023. Epub 2021/04/07. https://doi.org/10.15252/msb.202010023 PMID: 33821563; PubMed Central PMCID: PMC8022201.

70. McConville MJ, Bacic A. A family of glycoinositol phospholipids from *Leishmania major*. Isolation, characterization, and antigenicity. J Biol Chem. 1989; 264(2):757–66. Epub 1989/01/15. PMID: 2910865.

71. Zamboni N, Fendt SM, Ruhl M, Sauer U. (13)C-based metabolic flux analysis. Nat Protoc. 2009; 4(6):878–92. Epub 2009/05/30. https://doi.org/10.1038/nprot.2009.58 PMID: 19478804.

72. Prinsen H, Schiebergen-Bronkhorst BGM, Roeleveld MW, Jans JJM, de Sain-van der Velden MGM, Visser G, et al. Rapid quantification of underivatized amino acids in plasma by hydrophilic interaction liquid chromatography (HILIC) coupled with tandem mass-spectrometry. J Inherit Metab Dis. 2016; 39(5):651–60. Epub 2016/04/22. https://doi.org/10.1007/s10545-016-9935-z PMID: 27099181; PubMed Central PMCID: PMC4987396.

73. Rahman K, Zhao P, Mandalasi M, van der Wel H, Wells L, Blader IJ, et al. The E3 Ubiquitin Ligase Adaptor Protein Skp1 Is Glycosylated by an Evolutionarily Conserved Pathway That Regulates Protist Growth and Development. J Biol Chem. 2016; 291(9):4268–80. Epub 2016/01/01. https://doi.org/10.1074/jbc.M115.703751 PMID: 26719340; PubMed Central PMCID: PMC4813455.

74. Barylyuk K, Koreny L, Ke H, Butterworth S, Crook OM, Lassadi I, et al. A Comprehensive Subcellular Atlas of the *Toxoplasma* Proteome via hyperLOPIT Provides Spatial Context for Protein Functions. Cell Host Microbe. 2020; 28(5):752–66 e9. Epub 2020/10/15. https://doi.org/10.1016/j.chom.2020.09.011 PMID: 33053376; PubMed Central PMCID: PMC7670262.

75. *The Plasmodium* Genome Database C. PlasmoDB: An integrative database of the *Plasmodium falciparum genome*. Tools for accessing and analyzing finished and unfinished sequence data. The Plasmodium Genome Database Collaborative. Nucleic Acids Res. 2001; 29(1):66–9. Epub 2000/01/11. https://doi.org/10.1093/nar/29.1.66 PMID: 11125051; PubMed Central PMCID: PMC29846.

76. Zhang M, Wang C, Otto TD, Oberstaller J, Liao X, Adapa SR, et al. Uncovering the essential genes of the human malaria parasite *Plasmodium falciparum* by saturation mutagenesis. Science. 2018; 360 (6388). Epub 2018/05/05. https://doi.org/10.1126/science.aap7847 PMID: 29724925; PubMed Central PMCID: PMC6360947.